ELSEVIER

New Astronomy 3 (1998) 175–218

NEW ASTRONOMY

Proposed noncryogenic, nondrag-free test of the equivalence principle in space

A.M. Nobili[a,1], D. Bramanti[a,2], G. Catastini[a,3], E. Polacco[b,4], G. Genta[c,5], E. Brusa[c,6], V.P. Mitrofanov[d,7], A. Bernard[e], P. Touboul[e,8], A.J. Cook[f], J. Hough[g,9], I.W. Roxburgh[h,10], A. Polnarev[h,11], W. Flury[i,12], F. Barlier[j,13], C. Marchal[e]

[a]*Gruppo di Meccanica Spaziale, Dipartimento di Matematica, Università di Pisa, Via F. Buonarroti 2, I-56127, Italy*
[b]*Dipartimento di Fisica, Università di Pisa, Piazza Torricelli 2, I-56100, Italy*
[c]*Dipartimento di Meccanica, Politecnico di Torino, Italy*
[d]*Department of Physics, Moscow State University, Russia*
[e]*ONERA, Chatillon, France*
[f]*Selwyn College, Cambridge, UK*
[g]*Department of Physics and Astronomy, University of Glasgow, UK*
[h]*Astronomy Unit, Queen Mary and Westfield College, London, UK*
[i]*ESOC, Darmstadt, Germany*
[j]*CERGA, Grasse, France*

Received 3 April 1997; accepted 9 September 1997
Communicated by Francesco Melchiorri

Abstract

Ever since Galileo scientists have known that all bodies fall with the same acceleration regardless of their mass and composition. Known as the *Universality of Free Fall*, this is the most direct experimental evidence of the *Weak Equivalence Principle*, a founding pillar of General Relativity according to which the gravitational (passive) mass m_g and the inertial mass m_i are always in the same positive ratio in all test bodies. A space experiment offers two main advantages: a signal

[1]E-mail: nobili@dm.unipi.it
[2]E-mail: bramanti@keplero.dm.unipi.it
[3]E-mail: catasti@dm.unipi.it
[4]E-mail: polacco@difi.unipi.it
[5]E-mail: genta@polito.it
[6]E-mail: brusa@polito.it
[7]E-mail: mitr@mol.phys.msu.su
[8]E-mail: touboul@onera.fr
[9]E-mail: hough@physics.gla.ac.uk
[10]E-mail: i.w.roxburgh@qmw.ac.uk
[11]E-mail: polnarev%starlink.qmw.ac.uk@ib.rl.ac.uk
[12]E-mail: wflury@esoc.esa.de
[13]E-mail: barlier@ocar01.obs-azur.fr

1384-1076/98/$19.00 © 1998 Elsevier Science B.V. All rights reserved.
PII S1384-1076(97)00049-3

about a factor of a thousand bigger than on Earth and the absence of weight. A new space mission named GALILEO GALILEI (GG) has been proposed (Nobili et al., 1995 [J. Astronautical Sciences, 43, 219]; GALILEO GALILEI (GG), PRE PHASE A REPORT, ASI (Agenzia Spaziale Italiana), September 1996) aimed at testing the weak Equivalence Principle (EP) to 1 part in 10^{17} in a rapidly spinning (5 Hz) drag-free spacecraft at room temperature, the most recent ground experiments having reached the level of 10^{-12} (Adelberger et al., 1990 [PhRvD, 42, 3267]; Su et al., 1994 [PhRvD, 50, 3614]). Here we present a nondrag-free version of GG which could reach a sensitivity of 1 part in 10^{16}. The main feature of GG is that, similarly to the most recent ground experiments, the expected (low frequency) signal is modulated at higher frequency by spinning the system, in this case by rotating the test bodies (in the shape of hollow cylinders) around their symmetry axes, the signal being in the perpendicular plane. They are mechanically suspended inside the spacecraft and have very low frequencies of natural oscillation (due to the weakness of the springs that can be used because of weightlessness) so as to allow self-centering of the axes; vibrational noise around the spin/signal frequency is attenuated by means of mechanical suspensions. The signal of an EP violation would appear at the spin frequency as a relative (*differential*) displacement of the test masses perpendicularly to the spin axis, and be detected by capacitance sensors; thermal stability across the test masses and for the required integration time is obtained passively thanks to both the fast spin and the cylindrical symmetry. In the nondrag-free version the entire effect of atmospheric drag is retained, but a very accurate balancing of the test bodies must be ensured (through a coupled suspension) so as to reach a high level of *Common Mode Rejection* and reduce the differential effects of drag below the target sensitivity. In so doing the complexities of a drag-free spacecraft are avoided by putting more stringent requirements on the experiment. The spacecraft must have a high area-to-mass ratio in order to reduce the effects of nongravitational forces; it is therefore a natural choice to have three pairs of test masses (in three experimental chambers) rather than one as by Nobili et al. (1995) [J. Astronautical Sciences, 43, 219] and the mission called GALILEO GALILEI [PRE PHASE A REPORT, ASI (Agenzia Spaziale Italiana), September 1996]. The GG setup is specifically designed for space; however, a significant EP test on the ground is possible – because the signal is in the transverse plane – by exploiting the horizontal component of the gravitational and the centrifugal field of the Earth. This ground test is underway. © 1998 Elsevier Science B.V.

PACS: 04.80.Cc; 07.87.+v; 07.10.Yg; 07.10.Fq
Keywords: Gravitation; Relativity; Space vehicles; Celestial mechanics, stellar dynamics; Instrumentation: detectors; Earth

1. Introduction

In his *"Discorsi e dimostrazioni matematiche ..."* published in Leiden in 1638 while he was blind and under house arrest in Italy (Galilei, 1638) Galileo reported results of experiments carried out almost forty years earlier with pendula and the inclined plane. He formulated with astonishing neatness what lately became known as the *Principle of Equivalence*, according to which all bodies fall in the same way regardless of their mass and composition: *... veduto, dico questo, cascai in opinione che se si levasse totalmente la resistenza del mezzo, tutte le materie descenderebbero con eguali velocità* (*... having observed this I came to the conclusion that, if one could totally remove the resistance of the medium, all substances would fall at equal speeds*). About 80 years after Galileo's first experiments Newton went further, actually recognizing the equivalence of *mass* and *weight*. Newton regarded this equivalence as so important that he devoted to it the opening paragraph of the *Principia*, where (Definition I) he stated: *"this quantity that I mean hereafter under the name of ... mass ... is known by the weight ... for it is proportional to the weight as I have found by experiments on pendulums, very accurately made ..."* (Cajori, 1934).

At the beginning of the 20th century, almost 300 years since Galileo's work, Einstein realized that because of the equivalence between the gravitational (passive) mass m_g and the inertial mass m_i (i.e. the weak equivalence principle), the effect of gravitation is locally equivalent to the effect of an accelerated frame and can be locally cancelled. In a freely falling system all masses fall equally fast, hence gravitational acceleration has no local dynamical effects. Eins-

tein then generalized the *weak equivalence principle* to the *strong equivalence principle*, on which he based his theory of General Relativity. The *strong equivalence principle* states that in an electromagnetically shielded laboratory, freely falling and non-rotating, the laws of Physics – including their numerical content – are independent of the location of the laboratory. In such a laboratory all particles free of nongravitational forces move with the same acceleration. That is to say, *the effects of gravity, according to General Relativity, are equivalent to the effects of living in a curved spacetime*. In this sense the weak equivalence principle expresses the very essence of General Relativity and as such it deserves to be tested as accurately as possible. In the last 30 years since the advent of the space age General Relativity has been subject to extensive experimental testing as never before in its first 50 years of existence, and so far it has come out having no real competitors (e.g. Will, 1992); the crucial area where experimental gravitation is likely to play an important rôle is in the verification of the weak equivalence principle itself, since it is tantamount to testing whether gravitation can be ascribed to a metric structure of spacetime.

The total mass-energy of a body is the sum of many terms corresponding to the energy of all the conceivable interactions and components: $m = \sum_k m_k$. For two bodies A and B of different composition the Eötvös parameter $\eta = 2[(m_g/m_i)_A - (m_g/m_i)_B]/[(m_g/m_i)_A + (m_g/m_i)_B]$ can be generalized into

$$\eta_k = \frac{(m_g/m_i)_{Ak} - (m_g/m_i)_{Bk}}{\frac{1}{2}[(m_g/m_i)_{Ak} + (m_g/m_i)_{Bk}]} \qquad (1)$$

such that a non-zero value of η_k would define the violation of equivalence between the inertial and gravitational mass–energy of the k-th kind. For instance, the rest mass would contribute (as a fraction of the total) for $\simeq 1$; the nuclear binding energy for $8 \cdot 10^{-3}$, the mass difference between neutron and proton for $8 \cdot 10^{-4}(A - Z)$ (A being the number of protons plus neutrons and Z the number of protons in the nucleus), the electrostatic energy of repulsion in the nuclei for $6 \cdot 10^{-4} Z^2 A^{-4/3}$, the mass of electrons for $5 \cdot 10^{-4} Z$, the antiparticles for $\simeq 10^{-7}$, the weak interactions responsible of β decay for $\simeq 10^{-11}$. From the point of view of conventional field theory, the verification of all these separate equivalence principles corresponds to a very peculiar coupling of each field to gravity; whether and why it should be so in all cases is a mystery. Let us consider the case of antiparticles. A peculiarity of gravity, strictly related to the Equivalence Principle (EP), is that there is so far no evidence for *antigravity*, namely for the possibility that matter is gravitationally repelled by antimatter. A negative ratio of inertial to gravitational mass would obviously violate the equivalence principle and forbid any metric theory of gravity. Yet, there are theoretical formulations which would naturally lead to antigravity (Scherk, 1979), and experiments have been proposed to directly explore the relation between gravity and antimatter. The idea is to make a Galileo-type mass dropping experiment using a proton and an antiproton in order to check whether they both fall like ordinary matter or not. The experiment was proposed to CERN by an international team of scientists (Beverini et al., 1986). Unfortunately, while experiments concerning the inertial mass of antiparticles have been highly successful, and these are very accurately known, gravitational experiments (i.e. involving the gravitational mass of antiparticles) are extremely difficult because of the far larger electric effects, such as those due to stray electric fields in the drift tube. Indeed, the latter have so far hindered the experiment mentioned above. In absence of such direct tests, an improvement by several orders of magnitude of current tests of the weak equivalence principle with ordinary matter would also be an important constraint as far as the relation between gravity and antimatter is concerned. Several models of elementary particles have been proposed in which there are new long range forces between neutral particles. Generally they lead to forces between two bodies proportional to the product of two quantum numbers – e.g. their barion numbers – and as such they violate the equivalence principle. However, their state of development is uncertain and at present experiments on the weak equivalence principle do

not have a precise theory to test and a corresponding target accuracy.

The best ground experiments to test the weak equivalence principle have employed one of the most sensitive devices in the history of Physics: the torsion balance (Eötvös et al., 1922; Roll et al., 1964; Braginsky & Panov, 1972). More recently, thanks to the debate on the so-called *fifth-force* raised by Fishbach et al. (1986), a series of revised torsion balance experiments has been carried out reaching an accuracy of about 1 part in 10^{12} (Adelberger et al., 1990; Su et al., 1994). The main novelty is that the torsion balance is rotating in order to modulate the signal at higher frequency.

The crucial advantage of an EP space experiment in low Earth orbit is that the driving signal *in the field of the Earth* is given by the entire value of its gravitational acceleration. At 520 km altitude this amounts to $GM_{\oplus}/R^2 \simeq 840\,\mathrm{cm\,s^{-2}}$ (G is the universal constant of gravity, $M_{\oplus}$ the mass of the Earth and R the orbital radius of the satellite) as opposed to a maximum value of $\simeq 1.69\,\mathrm{cm\,s^{-2}}$ for a torsion balance on the ground in the field of the Earth (at 45° latitude) and $\simeq 0.6\,\mathrm{cm\,s^{-2}}$ in the field of the Sun. In contrast a short range EP experiment has nothing to gain from going into space, since much bigger source masses are available on the ground. The scientific objective of the nondrag-free GG mission proposed here is to test the weak equivalence principle in low Earth orbit to 1 part in 10^{16}. This requires to measure the effects of a very small *differential* acceleration $a_{\mathrm{EP}} \simeq 8.4 \cdot 10^{-14}\,\mathrm{cm\,s^{-2}}$. An accuracy of 10^{-16} in η would be a four order of magnitude improvement with respect to the current best ground tests. Even with a further improvement of ground results (e.g. to an accuracy of 1 part in 10^{13}) space would still allow a great leap forward. In order to avoid complexity, increase reliability and reduce cost, the whole mission design is focused on – and optimized for – EP testing only. Therefore, it does not offer a variety of scientific objectives as it has become the case for STEP (Worden & Everitt, 1973; Worden, 1976, 1987; Barlier et al., 1991; Blaser et al., 1993, 1994, 1996) and as proposed for the gravity mission based on the so-called SEE (*Satellite Energy Exchange*) method (Sanders & Deeds, 1992). In addition the experiment is non-cryogenic, the advantage being that there is no need to operate a cryostat in space in a very delicate, small-force experiment in which perturbations from the cryostat itself should be accurately controlled.

The main features of the mission derive from a careful analysis of ground based experiments on one side and the zero-*g* space environment on the other. EP experiments in the laboratory have demonstrated the advantage of rotating the torsion balance. As for vibrational noise (the analog of seismic noise on the ground), work done within the VIRGO project now under construction in Pisa has led to the development of very efficient attenuators. GG employs spinning test masses as well as mechanical suspensions. In order to reduce tidal (purely classical) gravitational perturbations, the two test masses – in the shape of hollow cylinders – are placed one inside the other. A precursor of GG, designed as a co-experiment in a multipurpose spacecraft, has appeared in 1992 (Bramanti et al., 1992) but indeed the first proposal for an EP space experiment with a spinning apparatus goes back to 1970 (Chapman & Hanson, 1970). It must be realized that an EP experiment with spinning test masses can be severely limited by centrifugal forces. An important feature of GG is that, for the first time, it exploits the effect of self-centering of bodies in *supercritical rotation*. It is worth stressing that, while an EP violation signal is modulated at the spin frequency, the effects of a large number of perturbing forces (e.g. due to inhomogeneities of the test bodies, spacecraft mass anomalies, nonuniform thermal expansion, parasitic capacitances, etc.) appear as DC because the entire system is spinning.

Small force gravitational experiments in space usually need to be performed inside a spacecraft equipped with thrusters in order to compensate – to some extent and in the appropriate frequency range – for the effects of the residual atmosphere and/or solar radiation acting on its external surface (and not on the test bodies inside it). However, ordinary impulsive thrusters cannot be used because they would induce vibrations of the spacecraft also at the frequency of the signal. Proportional thrusters have therefore been studied, based either on appropriate

mechanical valves or on field emission electric propulsion (FEEP), but so far their in-flight performances have not been tested. Since the only scientific objective of GG is to test the equivalence principle, i.e. to detect any tiny difference in the gravitational attraction of the Earth on two bodies of equal mass and different composition, it is by definition a *differential experiment*. Hence, perturbations which produce the same effect on both test masses (*Common Mode Effect*) do not compete with the signal. If the masses are suspended (rather than free falling) any external drag effect will appear as an *inertial force* applied to their centres of mass and differ (for sufficiently equal masses) only because of differences in the suspension mechanisms. We have therefore devoted special care in devising a *coupled suspension* of the test bodies which allows us an accurate balancing and consequent reduction of the differential effects of inertial forces (*Common Mode Rejection*, CMR). Such a balancing would allow us to operate the experiment in non drag-free conditions, i.e. to retain entirely the perturbation from air drag (and solar radiation pressure) on the spacecraft while making small only the differential effects of the inertial forces that it generates on the suspended test bodies. Drag effects could be essentially eliminated without inducing vibrational noise were the experimental apparatus totally uncoupled from the spacecraft. This appears to be an interesting possibility in the case of a passive experimental apparatus; in fact it was proposed for measuring the universal constant of gravitation G with a miniature *planet-satellite* system inside an orbiting spacecraft (Nobili et al., 1990), and in general for measuring the effects of pure gravitational interaction of the test bodies (Sanders & Deeds, 1992). It is however much less attractive when dealing with an active apparatus which needs to get power from solar cells placed on the outer surface of the spacecraft and to be electrically discharged. In GG the thin springs which connect the laboratory to the spacecraft can be used for accommodating the required number of wires, and the fact of not having free floating masses avoids the build up of electrostatic charges.

In Section 2 we describe the spacecraft and the experiment. Section 3 shows, first in the framework of a simplified model and then with finite element numerical simulations, the advantages of supercritical rotation, the effect of self-centering and the concept of electrostatic active damping. Section 4 is devoted to tidal effects. The effects of inertial forces and the balancing procedure are discussed in Section 5. Thermal effects, thermal noise and the requirements on thermal stability (to be met by passive insulation) are computed in Section 6. The capacitance read out system is presented in Section 7; its sensitivity and the required level of balancing appear to be adequate for the experiment. Section 8 is devoted to showing that coupling with the higher mass moments of the test bodies from the monopole of the Earth and from nearby mass anomalies is sufficiently small. Section 9 deals with electrostatic and magnetic perturbations, reaching the conclusion that there is no need to reduce the magnetic field of the Earth inside the satellite. A procedure for locking the suspended masses during launch and properly unlocking them in orbit once the nominal spin rate has been reached is proposed in Section 10. A preprint of this paper is available (Nobili et al., 1994).

2. Experiment setup and orbit choice

2.1. The spacecraft, the experimental apparatus and the signal

In the present nondrag-free version of the mission the GG experiment is carried by a small, cylindrical, spin-axis stabilized spacecraft of about 60 cm base diameter, 70 cm height and 600 kg mass. The symmetry axis of the cylinder is, by construction, the axis of maximum moment of inertia so as to stabilize the rotation around it. The fact of not needing any active attitude control reduces the complexity of the mission and the experiment (see Section 2.2). The spacecraft is very compact (with an area-to-mass ratio $A/M \simeq 7 \cdot 10^{-3}\,\mathrm{cm^2 g^{-1}}$) in order to make the effect of non-gravitational forces, such as air drag and solar radiation pressure, as small as possible. The orbit is almost circular, almost equatorial at 520 km altitude and the spin axis of the satellite is

almost perpendicular to the orbit plane. This maximizes the signal and makes it unnecessary to perform any attitude manoeuvres after the initial setup. The satellite is therefore very close to a truly *passive* one, which is extremely desirable when carrying out a small force experiment. The outer surface of the spacecraft is available for solar cells so as to generate the required power.

Inside the spacecraft it is possible to accommodate three experimental chambers, each one carrying a couple of test masses for an EP violation experiment. Fig. 1 (to scale) shows schematically how actual test masses of 10 kg each can be accommodated inside such a satellite. However, it is easier to understand the experiment in the case of a single experimental chamber, as shown in Fig. 2. Vibrational noise of the spacecraft around the spin/signal frequency is reduced by suspending the test masses inside a low noise laboratory (also of cylindrical shape and maximum moment of inertia with respect to the symmetry axis) which we call PGB (*Pico Gravity Box*). Inside PGB a very low noise level is attained by suspending it to the spacecraft with appropriate springs of low elastic constant k_{PGB} and low mechanical quality factor Q_{PGB}. Thanks to weightlessness a mechanical suspension can drastically reduce the vibrational noise of the spacecraft above a low threshold frequency as shown in Fig. 3.

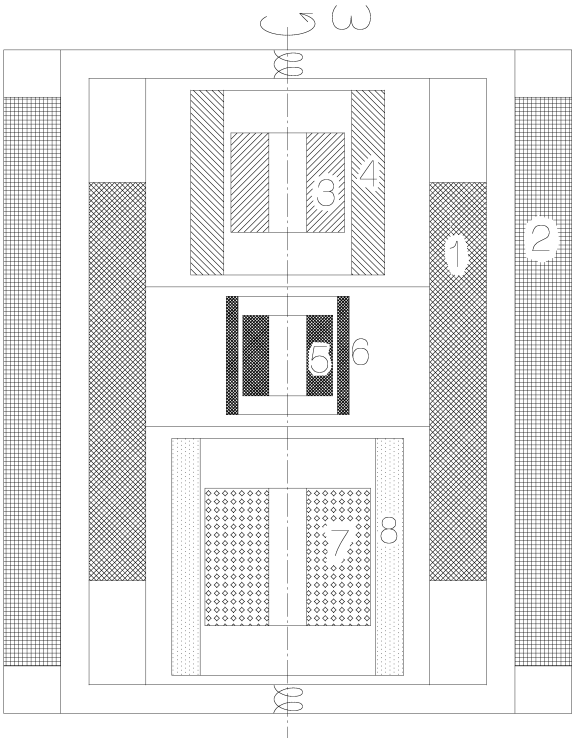

Fig. 1. Schematic section through the spin axis of the spacecraft showing the spacecraft, the suspended laboratory and the three experimental chambers containing two test masses each. The spacecraft is a cylinder of 70 cm height and 60 cm base diameter. The figure is to scale and shows that the experiment can be performed in a very small and compact satellite (the area-to-mass ratio is $7 \cdot 10^{-3}\,\mathrm{cm^2 g^{-1}}$). The central chamber contains two masses made of the same (dense) material for a null test. Each of the other two chambers contains two test masses of different materials, including low density ones. The numbers 1–8 are referred to in Section 3.

Passive mechanical suspensions in space for noise reduction in all six degrees of freedom have been the subject of recent extensive work (Nobili et al., 1991) in particular suspensions with low quality factor (which is very easy to obtain, e.g. with PTFE coating) in order to eliminate the resonance peaks (Catastini et al., 1992). The latter work gives an analytical model for longitudinal waves in a thin bar and shows that, with low Q, resonance peaks can be abated while maintaining a very good level of noise attenuation. Such a bar is not effective in the case of transverse waves. However, a mechanical suspension capable to respond with comparable stiffness in all directions (e.g. a helicoidal spring with a length comparable to its diameter) is suitable to reduce noise in all directions. If, in addition, it has a low Q value (for all types of deformations) it will also damp the resonance peaks. In the case of helicoidal springs (other shapes can be suitable too) one can play with the number of turns, their diameter, the way springs are fastened at their ends, the cross section of the wire and the total length of the spring in order to get (for a given spring material) the same, low, longitudinal and transversal elastic constant. If care is taken in using suspensions which have elastic and damping constants of the same order in all directions the analytical model used by Catastini et

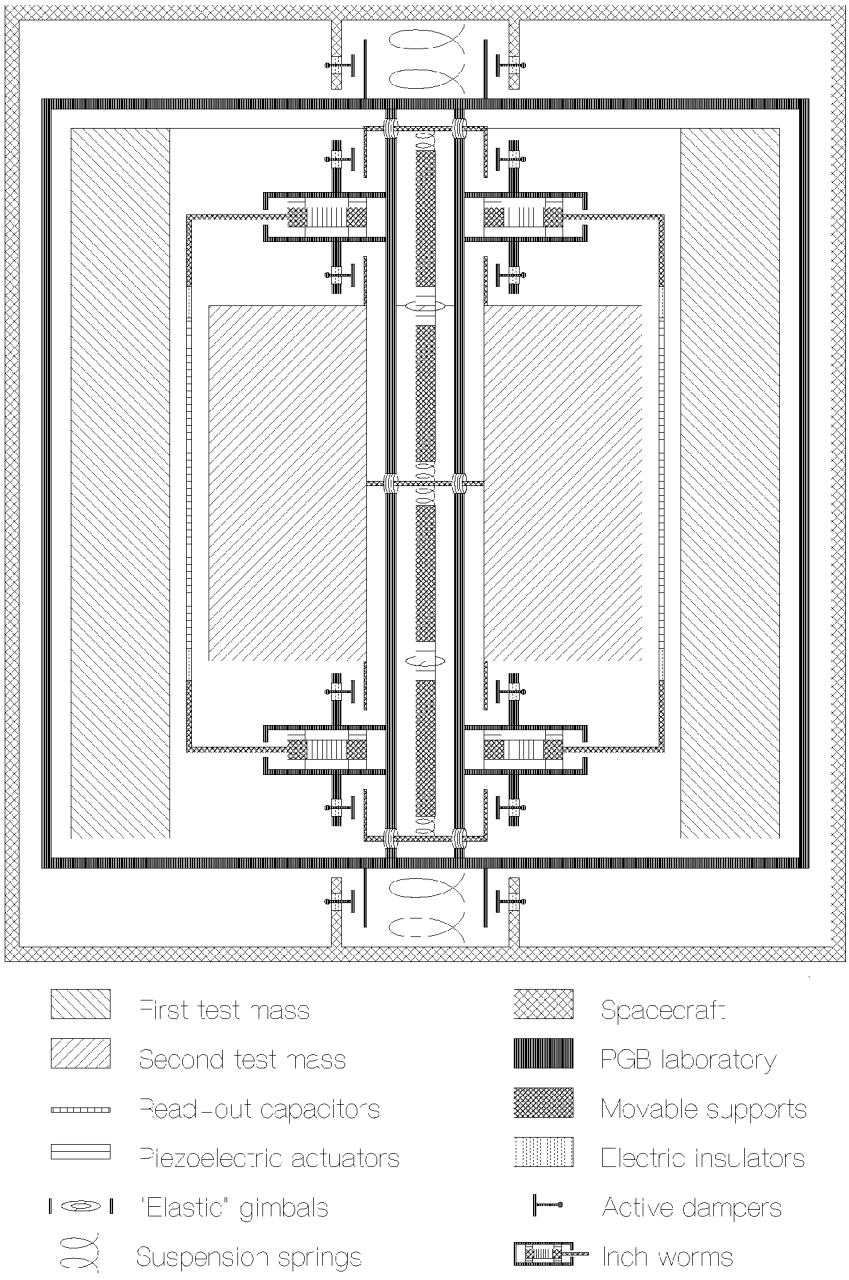

Fig. 2. Section through the spin axis of the spacecraft showing (not to scale) the spacecraft, the PGB laboratory and (for simplicity) only one experimental chamber. The PGB laboratory and the test masses are suspended with springs and their equilibrium positions can be stabilized by means of electrostatic active dampers (see Fig. 19 for a top view). The suspensions of the test masses also employ ''elastic'' gimbals (i.e. gimbals pivoted with torsion wires) on two movable rods for the balancing of inertial forces discussed in Section 5.2. The axial position of each half of these rods can be finely adjusted by means of piezoelectric actuators (see also Fig. 13). The capacitive plates of the read out system, between the test masses, are attached to inch-worms for adjusting their distance from the surfaces of the test masses.

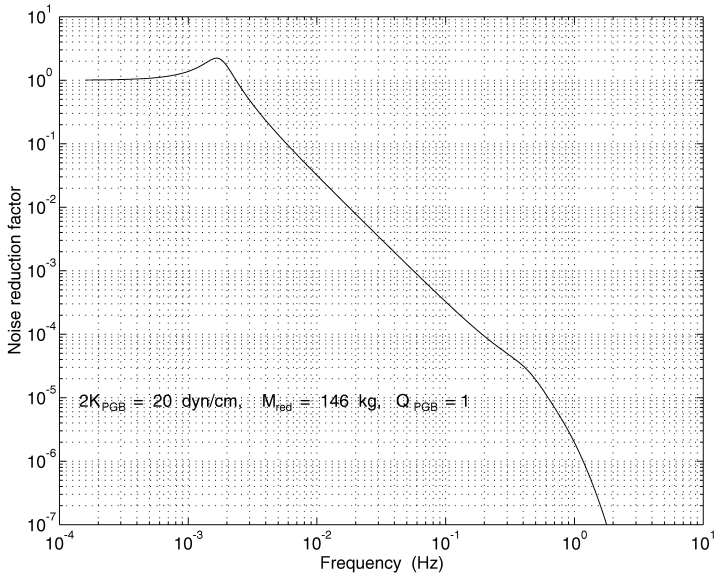

Fig. 3. Noise reduction factor (i.e. amplitude of disturbing vibration at the suspended mass over amplitude of vibration at the suspension point) as function of frequency for a suspended laboratory of 247.6 kg and mechanical suspensions with stiffness 10 dyn cm^{-1} and quality factor of order 1. $M_{\rm box}$ and all the rest of the system (spacecraft plus test masses).

al. (1992) is a good indication of what should be expected (Catastini et al. (1992) investigate also the problem of rotational noise showing that it is easier to deal with than the translational one). Laboratory work performed within the VIRGO project has shown that vibrational noise attenuation and damping can be extremely effective even in the more difficult 1-*g* environment. In order to appreciate the effectiveness and simplicity of a passive noise attenuator in space it is enough to notice that – except during the initial launch phase – the largest acceleration on GG, which is due to friction with the residual atmosphere, is smaller than the local gravitational acceleration on the Earth by a factor 10^9, which means that one can suspend 100 kg in space inside the GG spacecraft using the same (hair like) springs that one would use for suspending 0.1 milligram in a ground laboratory. Just to give an idea, an elastic constant of $\simeq 10$ dyn cm^{-1} (both transversal and longitudinal) is obtained with helicoidal springs a few cm long made of a few tens of turns each one of cm size and made with a wire of about 100 μm diameter. If the spring is coated with PTFE – in order to provide a low quality factor – a transfer function for vibrational noise like the one given in Fig. 3 can be obtained. This analysis has been extended to including the rotation of the spacecraft (Catastini et al., 1996).

It is important to note that the suspension springs of the PGB laboratory, besides ensuring a very low level of platform noise for the experiment, serve also other important purposes. The first is that, with no free floating masses no electrostatic charges will be able to build up anywhere inside the spacecraft. The second is to allow transferring the electric power generated by the solar cells to the experimental apparatus inside. The required number of wires can be accommodated either as independent helicoidal springs or by grouping them on a plastic support without any serious problem of degrading the reduction of vibrational noise. Once at the level of the PGB laboratory further transfer can take place through the rods and the gimbals (see Fig. 2).

An EP violation in the field of the Earth results in a *differential* force between the test masses in the

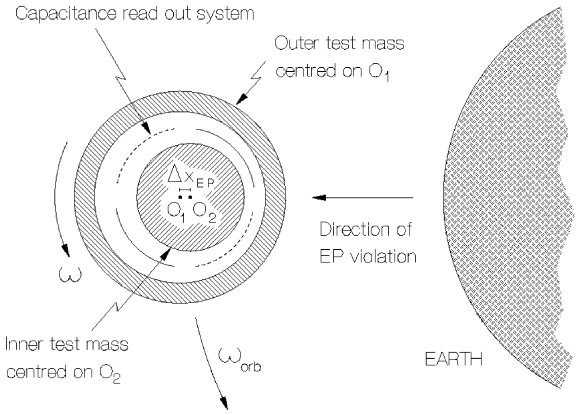

Fig. 4. Section across the spin axes of two test bodies with their centres of mass displaced by a distance Δx_{EP} due to an equivalence principle violation η in the field of the Earth. For $\eta = 10^{-16}$ (and with mechanical properties as given in Section 3.2) we get $\Delta x_{EP} \simeq 2.10 \cdot 10^{-10}$ cm. The centres of mass of the two bodies rotate independently around O_1 and O_2 respectively. The direction of the displacement Δx_{EP} changes with respect to inertial space as the satellite orbits around the Earth in 5700 s.

Earth-to-satellite direction which displaces their centres of mass to a new equilibrium where the EP violation force and the restoring force of the suspensions balance each other. At 520 km altitude the differential acceleration of an EP violation at the level $\eta = 10^{-16}$ is $a_{EP} \simeq 8.4 \cdot 10^{-14}$ cm s^{-2}. Each test body has mass $m \simeq 10$ kg and is suspended (like the PGB laboratory) by means of two springs with transversal and longitudinal stiffness $k = 10$ dyn cm^{-1} (Fig. 2). Two rods pivoted on elastic gimbals for each pair of test masses couple the two bodies to one another. The equivalent transverse elastic constant, as derived from the computed natural frequencies (Section 3.2) is $k_{eq} \simeq 4$ dyn cm^{-1}, hence the relative displacement caused by an EP violation with $\eta = 10^{-16}$ is $\Delta x_{EP} = m a_{EP}/k_{eq} \simeq 2.10 \cdot 10^{-10}$ cm (Fig. 4). Since the displaced equilibrium position is fixed in the Earth-to-satellite direction while the capacitance sensors are spinning, they will modulate this signal at their spin frequency, namely the spin frequency of the spacecraft. In this way the signal is displaced to a higher frequency (by several orders of magnitude) whereby reducing the effect of $1/f$ noise. We choose for the spin frequency the value of 5 Hz because it is large enough as compared to the threshold frequency of the noise attenuator to guarantee very good noise reduction, and yet reasonable for a spin-axis stabilized, small and compact satellite (note, for instance, that the european meteorology satellites METEOSAT, whose cylindrical body is more than 3 times bigger in height and diameter, spin at about 2 Hz). The capacitance bridge is adequately balanced so that common mode displacements at low frequencies, most importantly those at the orbital frequency of the spacecraft (e.g. due to air drag) will give signals always smaller than the *differential* signal expected from an EP violation (see Section 7). These common mode effects at low frequencies must also be adequately *rejected* (see Section 5.2) so that their residual *differential* effects will not compete with the expected signal. The fact that the entire system is spinning is extremely advantageous because it makes all effects caused by coupling to spacecraft mass anomalies and test masses inhomogeneities to appear as DC effects while the signal of interest is modulated at 5 Hz. The only moving mass on board will be a very limited amount of ordinary propellant which is needed only for the initial orbital and attitude adjustments before unlocking the test masses, and for redundancy. If the propellant is kept in a narrow toroidal tank close to the outer surface of the spacecraft, its motion will be dominated by the centrifugal force, thus ruling out a relative motion at the spinning frequency and therefore any interference with the signal.

In the GG setup, if the spin angular velocity vector $\boldsymbol{\omega}$ is at an angle θ with respect to the orbital angular velocity $\boldsymbol{\omega}_{orb}$ of the satellite around the Earth ($\omega_{orb} = \sqrt{GM_\oplus/R^3}$) the intensity of the differential displacement between the test masses as seen by the rotating sensors is of the form:

$$\Delta x = \Delta x_{EP} \cos(\omega t + \phi_{EP}) \cdot \mathcal{F} \qquad (2)$$

where $\Delta x_{EP} \simeq 2.10 \cdot 10^{-10}$ cm is the relative displacement of the suspended test masses in the satellite-to-Earth direction caused by an EP violation

with $\eta = 10^{-16}$ and ϕ_{EP} is the phase of the EP violation signal, which is known. The factor $\mathcal{F} = \cos\theta + \sin\theta\cos(\omega_{orb}t + \phi)$ comes into play in case the angle θ is not zero (ϕ is the phase angle of the sensors with respect to the satellite-to-Earth direction). If $\theta = 0$ (i.e. the spin axis is exactly perpendicular to orbit plane) $\mathcal{F} = 1$, whereas for any $0 < \theta \leq \pi/2$ this factor does reduce the intensity of the EP violation effect and introduces a dependence also on the orbital period of the satellite. This is why the spin axis of the satellite should be perpendicular to the orbit plane. It also leads to choosing an equatorial orbit for the satellite.

2.2. The orbit and the attitude

Because of the flattening of the Earth, the ascending node of a satellite orbit not exactly equatorial would regress along the equator, i.e. the normal to the orbit plane would describe a cone around the normal to the equator. The spin axis of the satellite, if not exactly normal to the orbit would in turn precess around the normal to the orbit because of the effect of the Earth's monopole on a body – the satellite – with different principal moments of inertia. Thus, even if the spin axis and the normal to the orbit were originally aligned, they would no longer be so after a few tens of days. Attitude manoeuvres would then be necessary to realign the spin axis to the orbit normal in order to have a factor $\mathcal{F} = 1$ in Eq. (2), hence to maximize the effect of an EP violation. This may require to activate the locking-unlocking device (Section 10), which would complicate the mission. Instead, if the satellite is originally injected in an orbit close to equatorial with the spin axis close to the normal to it, the spin axis and the orbit normal will stay close to one another (by the same amount) and attitude manoeuvres will not be required. In addition to that, the equatorial orbit has – if low enough – the advantage of avoiding the perturbing effects of the radiation from the Van Allen belts in the so-called South Atlantic Anomaly. An altitude of 520 km is suitable for this purpose. We therefore assume an equatorial, low eccentricity orbit at $\simeq 520$ km altitude and allow for an angle of a few degrees between the spin axis and the normal to the orbit plane as well as the inclination of the orbit on the equator, which are rather relaxed constraints for orbit injection. In this configuration no active control is needed, neither of the attitude nor of the orbit.

The satellite should be equipped with ordinary star trackers or Earth elevation sensors in order to monitor its spin rate and its instantaneous orientation. Although a predetermined spinning frequency is not needed, a knowledge of the actual spin rate or, more precisely, of the angle ϕ at all times, is required in the process of data analysis for removing small perturbations close to the signal frequency (Section 5.3), for checking purposes and to provide the electrostatic damper with a reference signal synchronized to the spin (Section 3.1). For communication with the Earth several choices are possible (see GALILEO GALILEI, 1996); a despun antenna should be avoided because moving parts would disturb the experiment. Since the orbit is low and equatorial the satellite will be in view of the ground station only for a fraction of its orbital period. There is no special need for continuous tracking; the experimental data can be stored on board and down loaded once per orbit. The required bit rate is low.

2.3. EP violation signal driven by the Sun and other sources

While moving around the Earth the test masses will also orbit, together with the planet, around the Sun. Therefore, the equivalence between inertial and gravitational mass can also be tested by comparing the gravitational attraction of the Sun with the centrifugal force due to the orbital motion around it. In this case the acceleration of an EP violation is $a_\odot \simeq (GM_\odot/d^2_{\oplus\odot})\eta_\odot$, with $M_\odot$ the mass of the Sun acting at its distance from the satellite (in practice the Earth–Sun distance $d_{\oplus\odot}$, namely 1 AU), and $\eta_\odot$ the Eötvös parameter expressing the violation of the equivalence between inertial and gravitational mass for the test masses in the field of the Sun. Since $GM_\odot/d^2_{\oplus\odot} \simeq 0.6\,\mathrm{cm\,s^{-2}}$, while $GM_\oplus/R^2 \simeq$

$840\,\mathrm{cm\,s^{-2}}$ it is apparent that our experimental apparatus cannot detect an EP violation due to the Sun to the same accuracy as for the Earth. We shall have $\eta_{\odot} \simeq 1.4 \cdot 10^{3}\eta$. For instance, if the experiment is limited to $\eta = 10^{-16}$, an EP violation due to the Sun can be tested to $\eta_{\odot} \simeq 1.4 \cdot 10^{-13}$, which would be better than achieved on Earth so far. The signal on the sensors will have a frequency which differs from that of an EP violation signal in the field of the Earth by the orbital frequency of the satellite. It will also be modulated by the annual motion of the Earth around the Sun. The two frequencies, from the Sun and from the Earth, can therefore be distinguished.

Similarly, one can analyze the data searching for possible violations of the equivalence principle driven by other sources such as the galaxy. Naturally, the sensitivity that can be achieved will depend on the intensity of the driving signal in each case, which however for the Sun and other sources farther away will be the same as it is on the ground. Indeed, all efforts towards more sensitive ground apparata for testing the equivalence principle should be strongly encouraged because their contribution is unique at short range and very valuable over distances much bigger than the radius of the Earth.

3. Self-centering in supercritical rotation

An experiment which aims at testing the equivalence principle must be capable to detect tiny relative displacements of the test masses with respect to one another. However, spurious relative motions would appear, because of gravity gradients, were the centres of mass of the test bodies not accurately centred on one another. This is why the test masses must be concentric, as they are in STEP. In GG their cylindrical shape is not only a construction advantage; it is clearly dictated by the symmetry of the one axis rotation. The crucial question is: how, and to what accuracy, is mass centering obtained? The answer comes from a careful exploitation of weightlessness, which makes the mechanical system (spacecraft, PGB and test masses) a rotor in *supercritical rotation* with the spin frequency ω much larger than the natural oscillation frequency ω_{tm} of the suspended test masses (and the PGB laboratory as well). Since the end of last century such rotors are known to have an equilibrium position very close to the rotation axis, which is pivotal in reducing the otherwise destructive effects of centrifugal forces in high-speed machines such as turbines, centrifuges and ultra-vacuum pumps (see Whitley (1984) for a review). In simple terms, the rotor tends to spin around its centre of mass, i.e. it behaves more like a free rotor rather than a constrained one. If the centre of mass of the suspended body is located, by construction, at a distance ϵ from the rotation axis, equilibrium is established on the opposite side of ϵ with respect to the rotation axis, where the centrifugal force due to rotation and the restoring elastic force of the suspension equal each other. It can be shown that this happens at a distance from the spin axis *smaller* than the original unbalance ϵ by a factor $(\omega_{\mathrm{tm}}/\omega)^2$ (see, e.g., Ch. 6 of Den Hartog, 1985). Thus, at equilibrium, the distance Δx_{cc} of each suspended test mass inside the GG satellite from the spin axis – and therefore from one another – is:

$$\Delta x_{\mathrm{cc}} \simeq \left(\frac{\omega_{\mathrm{tm}}}{\omega}\right)^2 \cdot \epsilon \tag{3}$$

Since the pioneer work of Gustaf De Laval about a century ago this relationship has been widely demonstrated in both theoretical and experimental work on high speed rotors. It shows that space offers an important advantage, because in absence of weight the natural frequencies of suspended bodies can be very low, about 10^3 smaller that the spin frequency in this case. For an original unbalance $\epsilon \simeq 10^{-3}\,\mathrm{cm}$ this means that the equilibrium position is only $\simeq 10^{-9}\,\mathrm{cm}$ away from the spin axis. It is important to stress that this equilibrium position slightly displaced from the rotation axis is fixed in the rotating frame of the spacecraft while the signal is modulated at the frequency of spin. Possible imperfections on the surfaces of the bodies would also give a DC effect. The actual direction of the miscentering in the rotating system depends only upon the location of the unbalance and is of no importance for the experiment. Perturbations such as air drag and solar

radiation pressure acting on the external surface of the spacecraft produce a nongravitational acceleration of its centre of mass. In the reference frame of the spacecraft the bodies will therefore be subject to inertial forces in the opposite direction, which will move the masses to new displaced positions of equilibrium (along the direction of the perturbation) where the perturbation is balanced by the restoring force of the spring. It is worth noticing that, because of the supercritical state of rotation, the displaced body will always spin around its own axis, which means that no centrifugal force due to the spin will result because of this displacement. The only centrifugal forces due to the spin come from the Δx_{cc} miscentering given by Eq. (3) and are balanced by the restoring force of the suspension springs.

It is however well known that any rotating system operating in the supercritical regime is unstable – owing to its internal damping – unless an adequate ''non-rotating damping'' is applied to it, that is damping caused by friction of the non rotating – or slowly rotating – parts of the bearings (on which the spinning shaft is mounted) against their supports. See Bramanti et al. (1996), Nobili et al. (1996) for an analysis of the various types of friction. Since the spacecraft as a whole is rotating, there is no way of obtaining the required non-rotating damping except by increasing the complexity of the system with the introduction of a fixed or slowly rotating portion of it. A simpler solution is to place in between the various masses active elements able to simulate the behaviour of a non-rotating damper. In the language of automotive active suspension technology the device can be defined as a ''skyhook damper'' since it acts as a damper which in a way follows an inertial reference frame. In Section 3.1 we show the main properties of supercritical rotation and the rôle of internal and non-rotating damping in a simplified mathematical model of two masses connected with springs; then report the results of a finite element numerical simulation of the system in the 3-chamber setup of Fig. 1, giving all the unstable whirling modes of the system and showing how they are damped (Section 3.2). The electrostatic damper is discussed in Section 3.3.

Unlike GG, the STEP experiment has been based on the fact that its attitude be actively maintained fixed with respect to inertial space as well as drag-free (in angle) to a level compatible with the requirement on orbital drag-free, which turns out to be a very demanding requirement. In this way, with a considerable effort in accurate active control, an EP violation signal from the Earth would appear at the satellite orbital frequency ($\simeq 1.8 \cdot 10^{-4}$ Hz). However, since the signal frequency is the frequency of orbital motion around the Earth it is bound to be also the frequency of a number of dangerous perturbing effects (e.g from the South Atlantic Anomaly and from the on board Helium used to make the experiment cryogenic). More recently it has been proposed that the STEP spacecraft be spinning too, but only slightly faster than its orbital revolution around the Earth. The benefits of fast satellite spin could not be incorporated either in the first proposed rotating experiment (Chapman & Hanson, 1970). In that experiment centrifugal forces remain a major limitation because the test bodies are constrained to move along one diameter of the rotating platform, and it is well known that any such rotating system is always strongly unstable above the critical speed (Ch. 6, p. 228 of Den Hartog, 1985).

3.1. Simplified mathematical model

Let us first study the system in the simplified model of two axisymmetrical rigid bodies of masses m_1 and m_2, length $2l$, moments of inertia J_{p1} and J_{p2} with respect to their symmetry (polar) axis and J_{t1}, J_{t2} with respect to any transversal axis x, y. The bodies are coupled by two identical springs, each of radial stiffness k as shown in Fig. 5. By introducing the complex coordinates $z = x + iy$ and $\phi = \phi_y - i\phi_x$, where ϕ_y and ϕ_x are the rotation angles around the y and x axes (the minus sign allows to simplify the metrical form of the equations), the equation of motion for the lateral dynamics of the system is (Section 4.6 of Genta, 1993):

$$[M]\{\ddot{q}\} + ([C] - i\omega[G])\{\dot{q}\} + ([K] - i\omega[C_r])\{q\} = \{F_r\}\omega^2 e^{i\omega t} \quad (4)$$

where

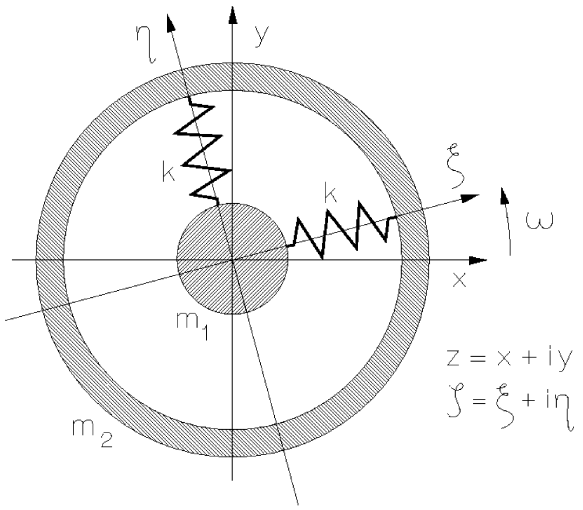

Fig. 5. A mathematical model of two axially symmetric bodies of masses m_1 and m_2 coupled by springs of stiffness k. x,y and ξ,η are the inertial and the rotating plane respectively. z and ζ are the complex variables in the two planes.

$$\{q\} = [z_1 \ \phi_1 \ z_2 \ \phi_2]^T$$

is the vector of the generalized coordinates of the system (subscripts 1 and 2 distinguish the two bodies) and $[M]$, $[G]$, $[K]$ are known as the mass, gyroscopic and stiffness matrices:

$$[M] = \begin{bmatrix} m_1 & 0 & 0 & 0 \\ 0 & J_{t1} & 0 & 0 \\ 0 & 0 & m_2 & 0 \\ 0 & 0 & 0 & J_{t2} \end{bmatrix},$$

$$[G] = \begin{bmatrix} 0 & 0 & 0 & 0 \\ 0 & J_{p1} & 0 & 0 \\ 0 & 0 & 0 & 0 \\ 0 & 0 & 0 & J_{p2} \end{bmatrix},$$

$$[K] = 2k \begin{bmatrix} 1 & 0 & -1 & 0 \\ 0 & l^2 & 0 & -l^2 \\ -1 & 0 & 1 & 0 \\ 0 & -l^2 & 0 & l^2 \end{bmatrix} \tag{5}$$

Because of possible construction errors each body will have the centre of gravity located a distance ϵ away from its rotation axis, and the symmetry axis tilted by an angle χ with respect to its rotation axis. These unbalances will result in the forcing terms at the right hand side of the equation of motion (Eq. (4)) which contain the vector $\{F_r\}$

$$\{F_r\} = [m_1\epsilon_1 e^{\alpha_1}(J_{p1} - J_{t1})\chi_1 e^{\beta_1} \times m_2\epsilon_2 e^{\alpha_2}(J_{p2} - J_{t2})\chi_2 e^{\beta_2}]^T \tag{6}$$

where α defines the direction of the vector $\boldsymbol{\epsilon}$ in the rotating frame and β is the phase angle of the couple due to the unbalance. In the general case of the Jeffcott rotor (Jeffcott, 1919) the system is subject to nonconservative forces (damping forces) which can be of two kinds: either of fixed direction in the inertial frame (non-rotating damping) or of fixed direction in the rotating frame (rotating damping). The latter occurs in the parts of the system which spin at speed ω (e.g. the springs), while the former is linked with the nonrotating parts of the machine. They are usually expressed as matrices $[C_n]$ and $[C_r]$ respectively, with $[C] = [C_n] + [C_r]$ the total damping matrix of the system. In the case of GG the entire system is spinning and therefore there is no nonrotating damping, i.e. $[C_n] = 0$ and $[C] = [C_r]$. The matrix $[C_r]$ is given by:

$$[C_r] = 2c \begin{bmatrix} 1 & 0 & -1 & 0 \\ 0 & l^2 & 0 & -l^2 \\ -1 & 0 & 1 & 0 \\ 0 & -l^2 & 0 & l^2 \end{bmatrix}$$

where c is the damping coefficient. For internal hysteretic damping the value of c, for the translational modes, can be approximated as $c = (1/Q)\cdot\sqrt{km_{\mathrm{eq}}/2}$, with Q the quality factor and $m_{\mathrm{eq}} = m_1m_2/(m_1 + m_2)$.

Because of symmetry Eq. (4) can be split into two different sets of uncoupled equations, one for the translational modes

$$\begin{bmatrix} m_1 & 0 \\ 0 & m_2 \end{bmatrix}\begin{Bmatrix} \ddot{z}_1 \\ \ddot{z}_2 \end{Bmatrix} + 2c\begin{bmatrix} 1 & -1 \\ -1 & 1 \end{bmatrix}\begin{Bmatrix} \dot{z}_1 \\ \dot{z}_2 \end{Bmatrix} + \left(2k\begin{bmatrix} 1 & -1 \\ -1 & 1 \end{bmatrix} - 2ic\omega\begin{bmatrix} 1 & -1 \\ -1 & 1 \end{bmatrix}\right)\begin{Bmatrix} z_1 \\ z_2 \end{Bmatrix} = \begin{Bmatrix} m_1\epsilon_1 e^{\alpha_1} \\ m_2\epsilon_2 e^{\alpha_2} \end{Bmatrix}\omega^2 e^{i\omega t} \tag{7}$$

and one for the rotational modes

$$\begin{bmatrix} J_{t1} & 0 \\ 0 & J_{t2} \end{bmatrix} \begin{Bmatrix} \ddot{\phi}_1 \\ \ddot{\phi}_2 \end{Bmatrix} + \left(2cl^2 \begin{bmatrix} 1 & -1 \\ -1 & 1 \end{bmatrix} - i\omega \cdot \begin{bmatrix} J_{p1} & 0 \\ 0 & J_{p2} \end{bmatrix} \right) \begin{Bmatrix} \dot{\phi}_1 \\ \dot{\phi}_2 \end{Bmatrix} + 2l^2 \left(k \begin{bmatrix} 1 & -1 \\ -1 & 1 \end{bmatrix} - ic\omega \cdot \begin{bmatrix} 1 & -1 \\ -1 & 1 \end{bmatrix} \right) \begin{Bmatrix} \phi_1 \\ \phi_2 \end{Bmatrix} = \begin{Bmatrix} (J_{p1} - J_{t1})\chi_1 e^{\beta_1} \\ (J_{p2} - J_{t2})\chi_2 e^{\beta_2} \end{Bmatrix} \omega^2 e^{i\omega t} \quad (8)$$

Let us consider the equation for the translational dynamics of the system (Eq. (7)). Assuming a solution of the type $z = z_0 e^{i\lambda t}$ for the free whirling, the characteristic equation of the homogeneous system is

$$\det\left(-\lambda^2 \begin{bmatrix} m_1 & 0 \\ 0 & m_2 \end{bmatrix} + 2ic\lambda \begin{bmatrix} 1 & -1 \\ -1 & 1 \end{bmatrix} + 2k \begin{bmatrix} 1 & -1 \\ -1 & 1 \end{bmatrix} - 2ic\omega \begin{bmatrix} 1 & -1 \\ -1 & 1 \end{bmatrix} \right) = 0 \quad (9)$$

whose solutions (i.e. the complex frequencies of the system) are 0 and the solutions of the equation:

$$-\lambda^2 \frac{m_1 m_2}{m_1 + m_2} + 2i(\lambda - \omega)c + 2k = 0 \quad (10)$$

which is the characteristic equation of a Jeffcott rotor with mass $m_{eq} = m_1 m_2/(m_1 + m_2)$ in the absence of non-rotating damping. It is well known that this device is unstable at all speeds exceeding the critical speed (see, e.g., 4.8.3 of Genta, 1993)

$$\omega_{cr} = \sqrt{\frac{2k}{m_{eq}}} \quad (11)$$

Thus, without non-rotating damping operation in supercritical regime (i.e. above the critical speed) is not possible because the rotor is necessarily unstable. From a more physical point of view, the springs – because of their internal dissipation – will necessarily transfer the spin angular momentum of each body to their rotational motion around one another, giving rise, in the inertial reference frame, to a circular forward motion of increasing amplitude of each axial end of the rotation axis of each body around the equilibrium position. There is a cylindrical whirl if the two ends move in phase and a conical (also called precessional) one if they move 180° out of phase. The natural position of equilibrium with the two axes very accurately aligned still exists but whirling motions around it necessarily grow in time, inevitably bringing the system to instability. It is worth stressing that if the suspension springs are very tiny, with very low stiffness k and relatively high Q values, the timescales of these instabilities are large, as numerical simulations confirm (Section 3.2). This is very important in devising an efficient active damper.

Non-rotating damping can be simulated by an active device which exerts on the mass m_1 a force

$$F = -c_a[(\dot{\zeta}_1 - \dot{\zeta}_2) + i\omega(\zeta_1 - \zeta_2)] \quad (12)$$

where c_a is the overall gain of the device and ζ is the complex displacement measured in the rotating reference frame ξ,η ($\zeta = \xi + i\eta$) as shown in Fig. 5. The device exerts a force of the same intensity and direction but opposite sign on the mass m_2. In the inertial reference frame x,y the equation of motion of the system is now given by Eq. (4) by adding the term

$$[C_n]\{\dot{q}\} \equiv 2c_a \begin{bmatrix} 1 & 0 & -1 & 0 \\ 0 & l^2 & 0 & -l^2 \\ -1 & 0 & 1 & 0 \\ 0 & -l^2 & 0 & l^2 \end{bmatrix} \begin{Bmatrix} \dot{z}_1 \\ \dot{\phi}_1 \\ \dot{z}_2 \\ \dot{\phi}_2 \end{Bmatrix}$$

to its left hand side. Assuming again a solution of the type $z = z_0 e^{i\lambda t}$ for the free whirling, the characteristic equation of the homogeneous system for translational motions is

$$\det\left(-\lambda^2 \begin{bmatrix} m_1 & 0 \\ 0 & m_2 \end{bmatrix} + 2i\lambda(c + c_a) \begin{bmatrix} 1 & -1 \\ -1 & 1 \end{bmatrix} + 2k \begin{bmatrix} 1 & -1 \\ -1 & 1 \end{bmatrix} - 2ic\omega \begin{bmatrix} 1 & -1 \\ -1 & 1 \end{bmatrix} \right) = 0 \quad (13)$$

whose solutions are 0 and the solutions of the equation:

$$-\lambda^2\frac{m_1m_2}{m_1+m_2}+2i\lambda(c+c_a)+2k-2i\omega c=0 \qquad (14)$$

which is the characteristic equation of a Jeffcott rotor with mass $m_{eq}=m_1m_2/(m_1+m_2)$, non-rotating damping c_a and rotating damping c. It is well known that this device is stable at all speeds below the maximum value ω_{max}:

$$\omega_{max}=\omega_{cr}\left(1+\frac{c_a}{c}\right) \qquad (15)$$

It follows that rotation at supercritical speed ω which were to ensure very good centering (i.e. $\omega \gg \omega_{cr}$) as well as stability necessarily requires $c_a \gg c$. The case of the test masses in the GG satellite is a very favourable one because the tiny suspension springs have very low internal damping c due to the very low stiffness k and relatively high Q. Hence a small amount of active damping c_a is sufficient to guarantee stability even at a spin frequency ω much larger than the critical frequency ω_{cr}. Thus, the active dampers are neither required to provide large forces nor to operate with small response times, since the unstable modes of the rotor are characterized by low frequencies (see Section 3.2). The nice fact about supercritical rotation is that the equilibrium position, with the axes closely aligned, is a physical property of the system and unstable rotational motions around this equilibrium position take place very slowly. This makes relatively easy centering to the position of equilibrium by means of active damping, clearly much easier than it would be in absence of such a naturally provided position of equilibrium. In Section 3.3 we present an electrostatic damper that appears to be suitable for our purposes. Here we wish to stress that in the rotating reference frame (to which the electrostatic plates of the damper are attached as shown in Fig. 2) it must supply a force with components:

$$\begin{cases} F_\xi = -c_a[(\dot\xi_1-\dot\xi_2)-\omega(\eta_1-\eta_2)] \\ F_\eta = -c_a[(\dot\eta_1-\dot\eta_2)+\omega(\xi_1-\xi_2)] \end{cases} \qquad (16)$$

Thus, since the effect produced by the damper must be at the frequency of the whirling motions, the unstable ones being at the (slow) natural frequency of oscillation, the damper must actuate at the spin frequency minus the natural one, which is different from the frequency of an EP violation. For the electrostatic plates to be able to recover and damp the slow velocity of whirl while spinning much faster, the control software must be able to subtract away their own velocity of spin, and this requires that either star trackers or Earth elevation sensors provide a reference signal synchronized with the spin. (For a detailed discussion on unstable whirl motions and active rotating damping in space see Bramanti et al., 1996; GALILEO GALILEI, 1997; Nobili et al., 1996).

3.2. Finite element model (FEM) numerical analysis

A more realistic model was built using the finite element rotordynamics code DYNROT, developed over the years at the Department of Mechanics of ''Politecnico di Torino''. The model, which includes the satellite body, the PGB laboratory and three pairs of test masses, is shown in Fig. 1 where the numbers 1–8 distinguish the various components of the system for later reference. The test masses are connected to the PGB by very low stiffness springs and movable supports with elastic gimbals at their midpoints as shown in Fig. 2. We first compute the whirling modes of the system assuming that no active dampers are present. The model consists of 36 beam elements and 20 spring elements (see Figs. 6,7). A number of beam elements which is larger than the minimum necessary to model the 8 cylindrical bodies and the central rod with movable supports has been used in order to allow us to define the location of the attachment points of the springs. The stiffness of the beam elements is orders of magnitude larger than that of the springs, so that they behave as rigid bodies in the whole frequency range of interest. Beam elements have been chosen instead of concentrated mass elements in order to use the ability of the code to compute directly the inertial properties from the geometrical parameters. Once the model was built, the number of degrees of freedom was reduced

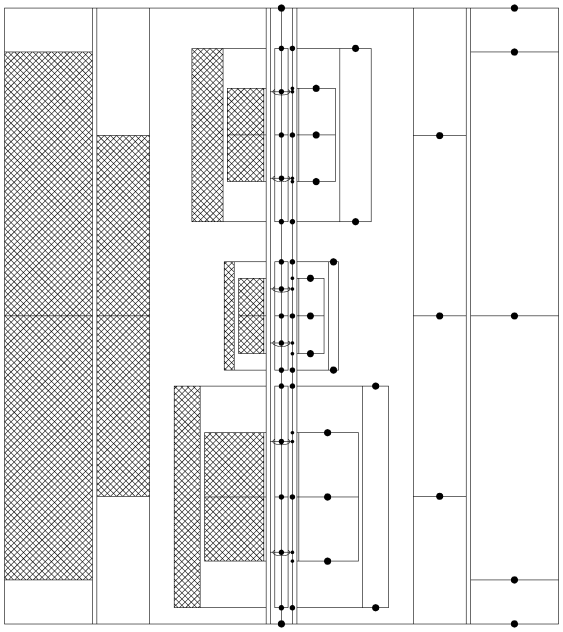

Fig. 6. Sketch of the FEM (Finite Element Method) model of GG. The figure shows the final FEM model used to analyse the rotordynamics of the active controlled system with DYNROT. The beam elements have been drawn on the left side of the picture: the white parts correspond to zero mass beams with structural stiffness. The nodes are shown on the right side of the sketch, each node corresponding to two translational and two rotational degrees of freedom which describe the lateral dynamics. In order to provide an understandable overview each node has been located on the corresponding beam element, instead of on the rotation axis of the satellite, as it actually is. Since each active damper has been connected to the central rod there are shorter beam elements near the gimbals and two nodes very close to each other.

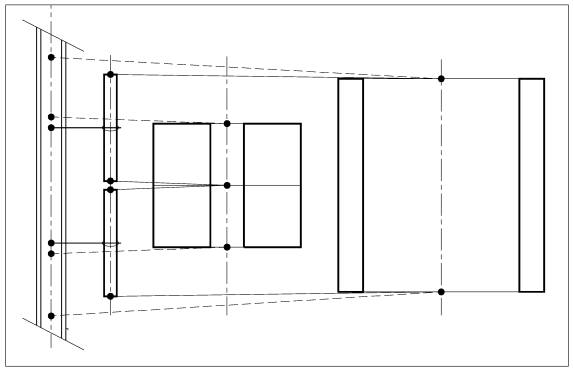

Fig. 7. Schematic representation of the various components of one experimental chamber placed next to one another in order to show the different kind of connections between them (springs, gimbals and electrostatic dampers). The outer and the inner test mass are respectively connected by spring elements (continuous line) to the pair of movable supports. Gimbals join the movable supports to the central rod, while the electrostatic dampers act between the test masses and the central rod (dotted line).

from 98 complex degrees of freedom, related to the displacements and rotations of all 49 nodes, to 16 through Guyan reduction (see, e.g., Section 2.8 of Genta, 1993). The minimum number of degrees of freedom necessary to define rigid-body motion was chosen, thus ensuring that no deflection of the beam elements can occur. The inertial properties of the rigid bodies are listed in Table 1, where the numbers 1–8 refer to the various parts of the system as shown in Fig. 1. The ratio $(J_p - J_t)/J_t$ is also listed. The masses of the central rod and of the movable supports have been neglected. The code was run using the same stiffness of 10 dyn cm^{-1}, both longitudinal and transversal, for all the springs (2 for each body) and the same torsional constant $k_{\mathrm{tor}} =$ 40 dyn cm, for all the elastic gimbals (2 for each pair of test masses). This value can be obtained if the diameter of the wires in the gimbals is about 10 μm and their length from 1 mm to 2 mm. The stiffness of the springs is relevant in response to forces in common mode while the gimbals enter into play when a pair of coupled test masses is subject to a differential force, resulting in an equivalent transverse stiffness k_{tor}/l^2 (l is the length of the rod from the gimbal to the spring, that is the arm; l is between 3 cm and 6.3 cm in the 3-chamber model of Fig. 1). The resulting equivalent transverse stiffness are therefore not exactly the same, but they are all smaller than the 10 dyn cm^{-1} stiffness of the springs. In the code the system is simplified in that either the springs or the gimbals respond, depending on whether the motion is in common mode (both masses together) or in differential mode (one mass with respect to the other) respectively. While it is true that the gimbals do not affect common mode

motions, the springs play a rôle also in differential motions. However, they respond to differential deformations with a lower elastic constant (the bending constant) than they do in the case of transversal common mode deformations. How much smaller is computed by Den Hartog (Appendix, p. 429 of Den Hartog, 1985), for a beam, and the numerical factor is 4. In laboratory tests with helicoidal springs we have measured a factor 3. Each pair of suspended test bodies will therefore have a lower natural frequency for oscillations in differential mode and a higher one for those in common mode: $\omega_{\rm tm}^{\rm d.m.} = \sqrt{2k_{\rm eq}/(2m)} = \sqrt{k_{\rm eq}/m}$ and $\omega_{\rm tm}^{\rm c.m.} = \sqrt{2k/m}$ (where $k_{\rm eq}$ is the equivalent transverse stiffness and k the stiffness of each spring; $2k$ because there are two springs for each mass and m because the reduced mass between the test mass m and the rest of the spacecraft is essentially m). A factor about 2 between these frequencies is reasonable to obtain, and this is the situation simulated with the DYNROT code.

The frequencies of free whirling are computed for the spacecraft spin rate $\omega = 31.4\,{\rm rad\,s^{-1}}$. Apart from the zero frequency modes, we find (in $\rm rad\,s^{-1}$): a set of 7 backward mainly conical whirling modes of frequencies $4.665 \cdot 10^{-5}$, $4.185 \cdot 10^{-5}$, $3.782 \cdot 10^{-5}$, $1.435 \cdot 10^{-5}$, $1.289 \cdot 10^{-5}$, $1.097 \cdot 10^{-5}$ and $6.463 \cdot 10^{-6}$; a set of 7 cylindrical modes, forward and backward of frequencies 0.0116, 0.0187, 0.0220, 0.0273, 0.0374, 0.0386 and 0.0426; a set of 8 conical forward whirling modes of frequencies 33.00, 33.13, 33.20, 33.37, 33.54, 34.11, 34.41, 36.70 close to the spin frequency. A graphical representation for some of the computed modes is given in Fig. 8. With the introduction of some internal damping of the springs which suspend the test masses (e.g. $Q \simeq 500$) it is found that only the forward cylindrical modes become unstable, and the e-folding times are a few 10^4 s (all other modes are naturally damped). As expected, instabilities are there but they build up slowly. As for the PGB laboratory the timescales for instability are shorter because, although the mass is bigger than that of the test bodies, the quality factor $Q_{\rm PGB}$ of its springs is smaller. Note that *all* modes with eigenfrequencies close to the spin/signal frequency are conical (i.e. angular precessions), not

Table 1
Inertial properties of the rigid bodies (as numbered in Fig. 1) which constitute the FEM model

Body #	m [10^3 g]	J_t [10^7 g cm^2]	J_p [10^7 g cm^2]	$(J_p - J_t)/J_t$
1	247.6	7.591	8.246	0.086
2	279.7	18.56	20.34	0.096
3	10	0.0378	0.0402	0.064
4	10	0.112	0.117	0.045
5	10	0.0130	0.0138	0.062
6	10	0.0303	0.0355	0.170
7	10	0.0199	0.0210	0.055
8	10	0.0694	0.0741	0.068
Σ	587.4	28.13	28.89	0.027

m is the mass; J_p is the moment of inertia with respect to the symmetry axis; J_t is the moment of inertia with respect to any transversal axis.

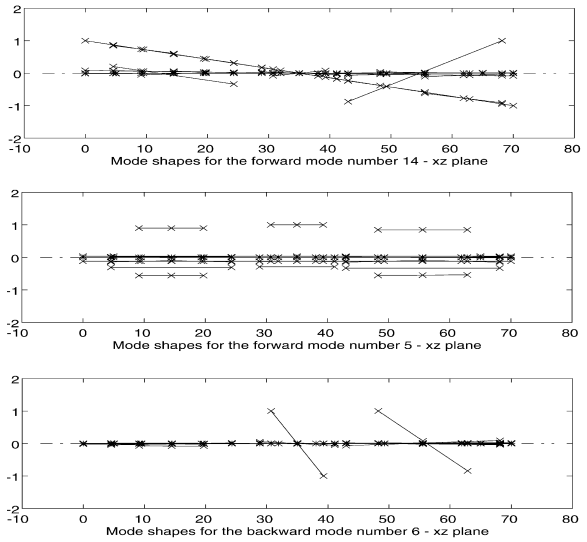

Fig. 8. Mode shapes of GG satellite. The mode shapes found by the DYNROT FEM code can be divided into three types: the first includes 7 cylindrical modes forward and backward, the second 7 backward mainly conical modes and the third 8 conical forward modes. A sample of each set including the 5$^{\rm th}$ and 14$^{\rm th}$ forward modes and the 6$^{\rm th}$ backward mode is shown by giving the position of the axis of rotation (continuous line) and the location of the nodes (the "×" symbols). The *x-axis* is a coordinate along the spacecraft axis (in cm); the *y-axis* is an adimensional normalized coordinate (the mode automatically scales all the modes to the maximum value).

cylindrical modes, which means that they do not affect the centre of mass of the bodies whose relative displacement is the observable in this experiment. Moreover, it is well known and the simulations confirm it, that they are naturally damped, i.e they are not unstable. We can conclude that there is no interference between these modes and the signal. As for the frequencies of the 7 cylindrical modes listed above (both forward and backward, the forward ones being those which become unstable in the presence of a nonzero internal damping of the springs) we note that they are the eigenfrequencies of the suspended bodies (two for each pair of test masses plus one for the PGB laboratory) as they have been computed in the numerical simulation of the 3-chamber system. As a matter of fact, since we study the mechanical system as a whole these are the natural frequencies of *the system*; however, due to the weakness of the springs, they can be still recognized as due to the various suspended masses. In order to avoid mutual mechanical influences between the three pairs of masses it is sufficient that their frequencies be separated by a few times their bandwidths. In this simulation in which all the springs have a stiffness of $10\,\mathrm{dyn\,cm^{-1}}$ and all the gimbals have a torsional constant of 40 dyn cm the DYNROT code provides: a frequency of about $0.0116\,\mathrm{rad\,s^{-1}}$ to be associated with the oscillations of the PGB and corresponding to an elastic constant $2k_{\mathrm{PGB}} \simeq 19.6\,\mathrm{dyn\,cm^{-1}}$; three frequencies between $0.019\,\mathrm{rad\,s^{-1}}$ and $0.027\,\mathrm{rad\,s^{-1}}$ to be associated with the differential modes; three higher frequencies between $0.037\,\mathrm{rad\,s^{-1}}$ and $0.043\,\mathrm{rad\,s^{-1}}$ to be associated with the common modes. From now on we use $3.95 \cdot 10^{-2}\,\mathrm{rad\,s^{-1}}$ for the common mode and $2.0 \cdot 10^{-2}\,\mathrm{rad\,s^{-1}}$ for the differential mode, noticing that there is enough liberty in the choice of the springs and gimbals to actually obtain these values. The corresponding elastic constants are: $k_{\mathrm{eq}} \simeq 4\,\mathrm{dyn\,cm^{-1}}$, for the response to forces in differential mode and $2k \simeq 15.6\,\mathrm{dyn\,cm^{-1}}$ for the response of each mass to forces in common mode. The fact of having a good separation between the eigenfrequencies in common mode and those in differential mode (the latter being smaller) is very useful because in this way displacements in response to perturbations in common mode (air drag) are reduced while those in differential mode (EP violation) are increased.

At this point we insert into the model a set of ideal active dampers providing the force (Eq. (16)). In doing so we also refine the model by increasing the number of elements to 82 (48 beam elements, 20 spring elements and 14 active dampers). The model includes 61 nodes and the number of degrees of freedom is reduced from 122 complex degrees to 16 through Guyan reduction. We assume a gain of $1.25\,\mathrm{dyn\,s\,cm^{-1}}$ for all the 12 elements damping the test masses. It is found that all unstable modes become stable and the timescales for damping are of 1 to 10 hours. For details on the physics of unstable whirl motions and their active control with rotating electrostatic dampers see Bramanti et al. (1996), GALILEO GALILEI (1997), Nobili et al. (1996).

3.3. The electrostatic damper

The force acting between the two elements of the electrostatic damper (Fig. 9) for an assumed voltage V is (in MKS):

$$F = \frac{\epsilon_\circ S}{2}\frac{V^2}{x^2} \tag{17}$$

with S the surface of the actuator and x the gap between the equipotential surfaces of the damper. For small displacements and tensions the force can be linearized around a constant voltage $V_\circ$ and reference gap $x_\circ$ for a superimposed control voltage V_c yielding

$$F_{x_{\mathrm{lin}}} = -2\epsilon_\circ S\frac{V_\circ}{x_\circ^2}V_c + 2\epsilon_\circ S\frac{V_\circ^2}{x_\circ^3}x \tag{18}$$

The second term on the right hand side describes the behaviour of a spring element with negative stiffness, and this must be softer than the mechanical springs: those linking PGB to the spacecraft body and those connecting each test masses to the central rod. The actuator is driven by a power amplifier modulated by the controller output signal. It provides the control voltage V_c to the capacitive load consti-

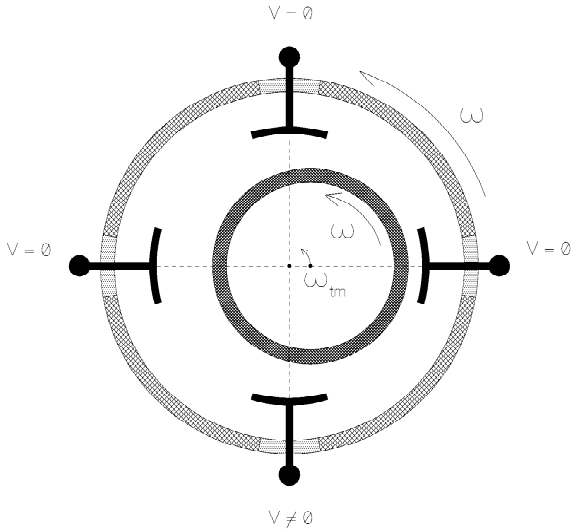

Fig. 9. Electrostatic damping of whirling motions. The circular instability motions of the rotation axis of the inner shaft, which have the natural (low) frequency of the suspended masses ω_{tm}, can be actively damped by means of the electrostatic force obtained by applying a voltage pulse V of short duration (for example for about one fourth of the spin period, i.e. about 0.05 s) to each plate rotating at the (rapid) spin frequency ω when it is passing through the position 90° before the point of its nearest approach to the inner shaft. This happens, for each plate, at a frequency which is equal to the spin frequency ω minus the natural frequency ω_{tm}.

tuted by the pair of electrostatic actuators. The resulting transfer function between the controller output signal V_u and the control voltage V_c is (the variable s indicates a Laplace transform with respect to time)

$$\frac{V_c(s)}{V_u(s)} = G_a(s) = \frac{k_a}{s\tau_a + 1} \tag{19}$$

with k_a the stationary gain and $1/\tau_a$ the power amplifier bandwidth. The transfer function between the displacement from the reference position of the rotor and the sensor output signal V_s, including the conditioning circuitry, is

$$\frac{V_s(s)}{x(s)} = G_s(s) = \frac{k_s}{s\tau_s + 1} \tag{20}$$

with k_s the stationary gain and $1/\tau_s$ the sensor bandwidth. In order to behave as required by Eq. (16) the controller must supply the output signals $V_{u\xi}$ and $V_{u\eta}$ for the plates acting respectively in ξ and η directions in accordance with the sensor outputs $V_{s\xi}$ and $V_{s\eta}$ in the same directions. The input-output relationships of the controller can be written in the form

$$\begin{Bmatrix} V_{u\xi} \\ V_{u\eta} \end{Bmatrix} = \begin{bmatrix} k_1 \dfrac{s}{s\tau_d + 1} & -k_2 \\ k_2 & k_1 \dfrac{s}{s\tau_d + 1} \end{bmatrix} \begin{Bmatrix} V_{s\xi} \\ V_{s\eta} \end{Bmatrix} \tag{21}$$

with k_1 and k_2 the stationary gains, and τ_d the time constant of the causal pole of the derivative term. By comparing Eqs. (16) and (21) it follows that the stationary gains of the controller must satisfy the relationships

$$k_2 = \omega k_1, \quad c_a = 2\epsilon_\circ S k_1 k_a k_s \frac{V_\circ}{h^2} \tag{22}$$

It is easy to verify that a gain $c_a = 1.25\,\mathrm{dyn\,s\,cm^{-1}}$ can be obtained with $S = 1\,\mathrm{cm}^2$, $h = 0.5\,\mathrm{cm}$, $V_\circ = 10\,V$, $k_1 = 14\,\mathrm{s}$, $k_s = 50\,V\,\mathrm{cm^{-1}}$ and $k_a = 25$. The negative stiffness of the electrostatic damper due to $V_\circ$ is $0.18\,\mathrm{dyn\,cm^{-1}}$, lower than the stiffness of the springs.

We have shown the feasibility of an electrostatic active damper with the characteristics required to ensure stability. The approximations introduced, particularly as far as the simulation of the electric circuit is concerned, are quite rough. Also, the dynamics of the sensors, controllers and power amplifiers has been neglected. However, the results are essentially correct because the frequencies at which the system works are quite low, orders of magnitude smaller than the characteristic frequencies of the electronic subsystems.

As for the thermal noise of the electrostatic active damper we have:

$$\frac{\Delta V_N}{\sqrt{\mathrm{Hz}}} \simeq \sqrt{4R_{\mathrm{eq}}K_B\overline{T}} \tag{23}$$

where $R_{\mathrm{eq}} = 1/(\omega_{\mathrm{ed}} C Q_{\mathrm{el}})$ is the equivalent resistance of the electrostatic damper of capacity $C = \epsilon_\circ S/h$ and

electric quality factor Q_{el} operated at frequency $\omega_{ed} \simeq 10^7 \,\mathrm{rad\,s^{-1}}$. Then,

$$\frac{\Delta V_N}{\sqrt{\mathrm{Hz}}} \simeq \frac{3 \cdot 10^{-4}}{\sqrt{\omega_{ed} Q_{el}}} \frac{V}{\sqrt{\mathrm{Hz}}} \tag{24}$$

Since the force exerted by the damper is $F = \epsilon_\circ V_\circ^2 S/(2h^2)$ ($V_\circ \simeq 10\,V$ the potential difference) the perturbing force corresponding to the noise is $\Delta F_N/\sqrt{\mathrm{Hz}} = \epsilon_\circ V_\circ \, \Delta V_N S/(h^2) \simeq 1.1 \cdot 10^{-13}/\sqrt{\omega_{ed} Q_{el}}\, N/\sqrt{\mathrm{Hz}}$. Dividing by the mass $m = 10\,\mathrm{kg}$ of the test body we get the perturbing acceleration:

$$\frac{\Delta a_N}{\sqrt{\mathrm{Hz}}} \simeq \frac{1.1 \cdot 10^{-14}}{\sqrt{\omega_{ed} Q_{el}}} \frac{\mathrm{m\,s^{-2}}}{\sqrt{\mathrm{Hz}}} \tag{25}$$

A comparison with the mechanical thermal noise (Section 6.2) shows that with a reasonable value of the electric quality factor $Q_{el} \simeq 10$, and $\omega_{ed} \simeq 10^7 \,\mathrm{rad\,s^{-1}}$ the contribution of each electrostatic damper to the thermal noise is negligible and it remains so even considering that the damping of each test body involves 8 capacitance plates. This result could be guessed from the fact that the force to be provided by each plate is very small. In point of fact we plan to confirm this result with experimental tests of the electrostatic damping system in the framework of a ground experimental test of the equivalence principle based, as GG, on supercritical rotation and mechanical suspension of concentric test cylinders.

Let us now estimate the amount of shot noise to be expected:

$$\frac{\Delta V_{SN}}{\sqrt{\mathrm{Hz}}} \simeq \sqrt{2 e V_{DC} R_{eq}} \tag{26}$$

where $e = 1.6 \cdot 10^{-19}\,C$ and $V_{DC} = i_{DC} R_{eq}$ is the potential difference due to the quantized current i_{DC}. With a capacity $C \simeq 1.8 \cdot 10^{-13}\,F$ for each electrostatic damper we get:

$$\frac{\Delta V_{SN}}{\sqrt{\mathrm{Hz}}} \simeq \frac{1.34 \cdot 10^{-3}}{\sqrt{\omega_{ed} Q_{el}}} \cdot \sqrt{V_{DC}} \, \frac{V}{\sqrt{\mathrm{Hz}}} \tag{27}$$

If $V_{DC} = 1\,\mathrm{V}$ (but usually is much smaller) the shot noise is about 5 times bigger than the thermal noise given by Eq. (24), which we have just seen to be negligible with respect to the mechanical thermal noise of the test masses.

4. Axial centering and Earth tides

We have seen in Section 3 that a position of relative equilibrium exists, naturally provided by the physics of the system, where the spin axes of the test bodies are extremely close to one another ($\simeq 10^{-9}$ cm in this case). It is worth recalling that the direction of this miscentering is fixed in the rotating system, its location depending on the direction of the original unbalance (by construction and mounting). We have also seen that slow (at the natural frequencies) whirl motions around this relative equilibrium can be damped by active electrostatic sensors/actuators rotating with the system. If the sensing errors allow them to detect displacements as small as the miscentering, the tidal perturbation (in the transverse plane), which is linear with the miscentering, is about 20 times smaller than the EP violation signal we are trying to measure. In case of higher sensing errors, the output signal can be analized to remove tidal variations at the natural frequencies.

The centres of mass of the test bodies could as well be a distance Δz away from one another along the axis itself, thus also giving rise to a tidal force. Were the spin axis exactly perpendicular to the orbit plane, the tidal force would have no component perpendicular to it. This not being exactly the case, such a component will appear, causing a relative displacement of the centres of mass with respect to one another. This tidal perturbation is, as in the case of an EP violation, a differential force directed towards the centre of the Earth slowly changing its direction as the satellite orbits the Earth. However, it can be distinguished from an EP violation signal and indeed used to drive a servo mechanism for reducing the vertical displacement Δz from its initial value of 10^{-3} cm–10^{-2} cm obtained by construction down to below the sensitivity of the experiment. This is possible for two reasons: i) Unlike EP violation,

these tidal forces have opposite directions on opposite sides of the Earth, depending on which mass is closer to the Earth (Fig. 10). This means that the tidal signal differs from an EP violation signal by the orbital frequency of the satellite, a difference which is detectable by measuring the spin rate of the spacecraft. ii) While the tidal force goes to zero with Δz, the EP violation force doesn't, i.e. mass centering does not change an EP violation signal.

If the spin axis is an angle θ away from the perpendicular to the orbit plane, and the bodies are at a distance Δz along the spin axis, the tidal acceleration on each test mass has a component perpendicular to the spin axis:

$$a_{\mathrm{ET}} \simeq \frac{3}{2}\frac{GM_{\oplus}}{R^3}\Delta z \sin 2\theta \simeq 1.8\cdot 10^{-6}\Delta z \sin 2\theta \ \mathrm{cm\,s^{-2}} \quad (28)$$

Allowing for an angle $\theta \simeq 1°$, this gives $\Delta z \simeq 1.3 \cdot 10^{-6}$ cm in order to have a perturbation to the level of the signal. With the capacitance read out system discussed in Section 7 it is no problem at all to detect miscentering down to the required value and use the piezoelectric actuators shown in Fig. 2 for active centering. Once the tidal acceleration signal has become too small to be detected it will also be too small to perturb the EP experiment. Using the tidal signal for axial centering of the test bodies was originally suggested for STEP (Worden et al., 1990). Besides the differential effect of Earth tides on the test masses, one must also consider the common mode tidal perturbation with respect to the centre of mass of the entire system. In particular, for the test bodies located inside the two experimental chambers above and below the centre of mass (Fig. 1), the distance Δz in Eq. (28) cannot be smaller than about 10 cm, thus resulting in a common mode tidal perturbation of about $6 \cdot 10^{-7}\,\mathrm{cm\,s^{-2}}$, also differing from an EP violation signal by the orbital frequency of the spacecraft (Fig. 10). An adequate level of common mode rejection is therefore necessary (see Section 5.2).

Fig. 10. Simple scheme of Earth tidal forces on two test bodies which rotate around the same axis but are displaced along it. The figure shows how the component of the tidal force towards the Earth changes phase by 180° every half orbital period of the satellite around the Earth. Only this component does produce a differential displacement of the centres of mass which can be recorded by the spinning capacitors. It is apparent that a differential force due to a violation of the equivalence principle would not change sign every 1/2 orbit and would not go to zero with the separation distance Δz.

5. Inertial forces

5.1. The common mode effect

The effect of nongravitational forces – such as air drag and solar radiation pressure – acting directly on the outer surface of the spacecraft and not on the suspended masses inside, is twofold. On one side they shake the spacecraft and produce vibrational noise whose spectral distribution covers a wide frequency range and depends on the particular spacecraft. This is not a matter of concern for the GG experiment thanks to the PGB mechanical suspension which is particularly effective at the 5 Hz frequency of the signal (Fig. 3). On the other side, nongravitational forces accelerate the satellite itself. Let us consider air drag, which at 520 km altitude dominates over solar radiation pressure (the effect of the Earth's albedo is even smaller). The main component of air drag is in the along track direction of the satellite with relatively large intensity variations and a slow change of direction over the orbital period of the satellite around the Earth. If the spacecraft is not designed to counteract air drag, it

will loose altitude and accelerate in the along track direction, with the result that the suspended bodies inside (the PGB laboratory as well as the test masses) will be subject to inertial translational forces. The lifetime of the satellite because of its orbit decay is $\simeq 40$ yr, by far longer than a few hours integration time needed for the EP experiment (Section 6.2) and also much longer than a reasonable mission duration which we foresee of several months to a year. The price we have to pay in order to avoid the complexity and cost of a sophisticated drag free system is exactly in the need to deal with these inertial translational forces. However, the first important fact to learn is that, unlike the forces which act directly on the surface of the spacecraft, inertial forces on the suspended bodies inside do not depend – *in any way* – on the surface properties of these bodies. Whatever the non gravitational acceleration on the satellite, the inertial force is simply given by the mass of the suspended body times this acceleration, it is centred at the centre of mass of the body and directed opposite to the nongravitational acceleration of the satellite. The balance between this force and the restoring force of the suspending spring gives the new position of equilibrium. Therefore, two suspended bodies with ideally equal masses and equal suspensions would be subject to exactly the same inertial forces: were they originally centred on one another with good enough precision for the EP experiment, they would continue to be centred on one another with the same precision in spite of air resistance acting on the spacecraft as well as of its variations.

This amounts to saying that the effect of the translational inertial forces on the suspended coaxial cylinders of the *GG* experiment is intrinsically common mode. Any difference that may arise, due to either a difference in the *masses* or a difference in the *suspensions*, will give a signal at the spinning frequency, i.e. the same frequency as the signal. However, they differ in phase as well as in the important property that while inertial differential forces go to zero with the relative differences in m and k (i.e. they can in principle be made zero by reducing $\Delta m/m$ and $\Delta k/k$ for the two bodies) the differential force due to an EP violation would still be there no matter how *equal* the masses of the test bodies and their suspensions are. The crucial question is therefore: How much do we need the inertial forces on the suspended test bodies to equal each other in order to be able to detect an EP differential acceleration $a_{\rm EP} \simeq 8.4 \cdot 10^{-14}\,{\rm cm\,s^{-2}}$ (i.e. $\eta = 10^{-16}$)? Making the signals equal is usually referred to as *Common Mode Rejection* (CMR). Given the goal in EP testing, the required CMR factor does depend on the value of the inertial force in common mode, hence on the intensity of the air drag acceleration on the spacecraft which we therefore try to keep as low as possible by making it small and compact. We have $A/M \simeq 7 \cdot 10^{-3}\,{\rm cm^2\,g^{-1}}$, the same as the area-to-mass of LAGEOS, the passive spherical satellite devoted to geodynamical studies. It is compatible with the 3-chamber setup of Fig. 1 and a total mass of about 600 kg. Once the orbiting altitude has been chosen the air density depends on the solar index, which changes with a period of $\simeq 11$ yr. We refer to data on atmospheric density provided by the GTDS (Cappellari et al., 1976), as function of the solar index and satellite altitude (a minimum and a maximum value are given for each altitude because of the nonspherical shape of the isodensity surfaces of the Earth atmosphere). The GTDS tables are based on the original atmospheric model of Harris & Priester (1952), (1962) which has been modified to include the dependence on the solar index and the asphericity of the atmospheric bulge. They are used by NASA and other space centres around the world for mission analysis and have been shown to be in very good agreement with the more recent and more sophisticated models (Jacchia, 1971; Roberts, 1971). If the mission is flown at 520 km altitude and the solar index is $F = 75$ (the solar index F in the GTDS tables goes from a minimum of 65 to a maximum of 275), the average air density is $\rho_{\rm atm} \simeq 2.04 \cdot 10^{-16}\,{\rm g\,cm^{-3}}$. The corresponding acceleration on the spacecraft is: $a_{\rm drag} \simeq (1/2) C_D (A/M) \rho_{\rm atm} v_{\rm sc}^2 \simeq 8.25 \cdot 10^{-7}\,{\rm cm\,s^{-2}}$, with $v_{\rm sc}$ the orbital velocity of the spacecraft and C_D its aerodynamic coefficient. The inertial common mode acceleration on the test masses is therefore $a_i^{\rm c.m.} \simeq 8.25 \cdot 10^{-7}\,{\rm cm\,s^{-2}}$ with

direction opposite to the drag acceleration. The equilibrium position discussed in Section 3 (where the centrifugal force due to the spin is balanced by the restoring force of the mechanical suspensions) will be displaced – in common mode – by an amount $\Delta r_i^{\mathrm{c.m.}} = m a_i^{\mathrm{c.m.}}/15.6 \simeq 5.3 \cdot 10^{-4}$ cm, each body spinning around its own axis displaced in the new position. Since the precise location of the laboratory, as well as the test bodies (in common mode!) is not needed, this displacement of the position of equilibrium – which is the main effect of the translational inertial forces – is no problem at all.

Indeed, the perturbation due to the air drag can be further reduced by flying the spacecraft at higher altitude: in going from 520 km to 600 km altitude the EP violation signal decreases only slightly while the drag effect is significantly reduced due to a much smaller air density. For instance, at 600 km altitude during a solar minimum ($F = 65$ in the GTDS tables) the maximum air density is $8.91 \cdot 10^{-17}\,\mathrm{g\,cm^{-3}}$, resulting in an acceleration on the spacecraft of $3.56 \cdot 10^{-7}\,\mathrm{cm\,s^{-2}}$, only slightly exceeding the perturbation due to the solar radiation pressure: $a_{\mathrm{rp}} = (\Phi_\odot/c)(A/M) \simeq 3.3 \cdot 10^{-7}\,\mathrm{cm\,s^{-2}}$ (with $\Phi_\odot$ the solar constant and c the velocity of light). This effect has a phase difference as well as a small relative difference in frequency with respect to an EP violation signal in the field of the Earth, as discussed in Section 2.3. The effect of Earth's albedo is smaller than the solar radiation effect because of the albedo coefficient of the Earth ($\simeq 0.3$); it also has an extremely clear signature because of its following the entering of the satellite in and out of the Earth's shadow.

5.2. Rejection of the common mode effect

The accuracy that can be achieved in the detection of an EP violation differential force relies crucially on the ability to reject the common mode effect of inertial forces on the test masses, which in turn is limited by the ability to balance the test bodies. This because it is much easier to make the masses equal than it is to equal the suspensions. As we have seen, the largest perturbation to compete with an EP violation signal is the inertial force resulting from air drag ($a_i^{\mathrm{c.m.}} \simeq 8.25 \cdot 10^{-7}\,\mathrm{cm\,s^{-2}}$), with the same frequency and 90° phase difference, while a 95% confidence level in the expected signal requires a sensitivity of $\simeq 4.2 \cdot 10^{-14}\,\mathrm{cm\,s^{-2}}$. If we show that a total common mode rejection by 10^{-7} can be achieved, so as to bring the differential effect of the inertial force due to air drag down to $a_i^{\mathrm{d.m.}} \simeq 8.25 \cdot 10^{-14}\,\mathrm{cm\,s^{-2}}$ then, since a factor 2 for the separation of effects with about 90° phase difference is generally accepted among experimentalists, we are below the required sensitivity (see Fig. 11).

As for the masses, 10 kg cylinders can certainly be made of equal mass to better than 1 part in 10^7. Making suspensions springs that are *equal* to 1 part in 10^7 and *stay equal* for the required integration time (see Section 6.2) and hopefully longer, is more difficult. First of all, we must distinguish between springs being *equal* and springs being *stable*. The problem of stable (helicoidal) springs has been widely investigated and techniques have been developed to reduce the release of accumulated stress. These include annealing as well as carving from a single piece of material. An important area of application for stable springs is in the construction of high sensitive gravimeters for accurate measurement of Earth tides (Melchior, 1978). In the 1-*g* environment, in absence of large shocks and temperature variations, gravimeters with metallic springs have reached an absolute drift value of of 1 part in 10^9 per day and a thermal stability of $(1/k)(\Delta k/\Delta T) \simeq 10^{-6}\,\mathrm{K^{-1}}$ (Melchior et al., 1979). These figures come from data recorded during a 1-yr (1978) measurement campaign at Alice Springs in Australia by P. Melchior, B. Ducarme and collaborators using the *Gravimètre 4084* (Melchior et al., 1979). It has been pointed out by Dr. Ducarme (Ducarme, 1994) that, although these figures are instrument dependent, drifts of 1 part in 10^8 per day are common in this field. This is encouraging, especially taking into account that gravimeters' springs on Earth are subject to deformations comparable to their length (along the direction of local gravity), while inside the GG spacecraft the largest acceleration is only $\simeq 10^{-9}$ g and the springs are deformed by less than

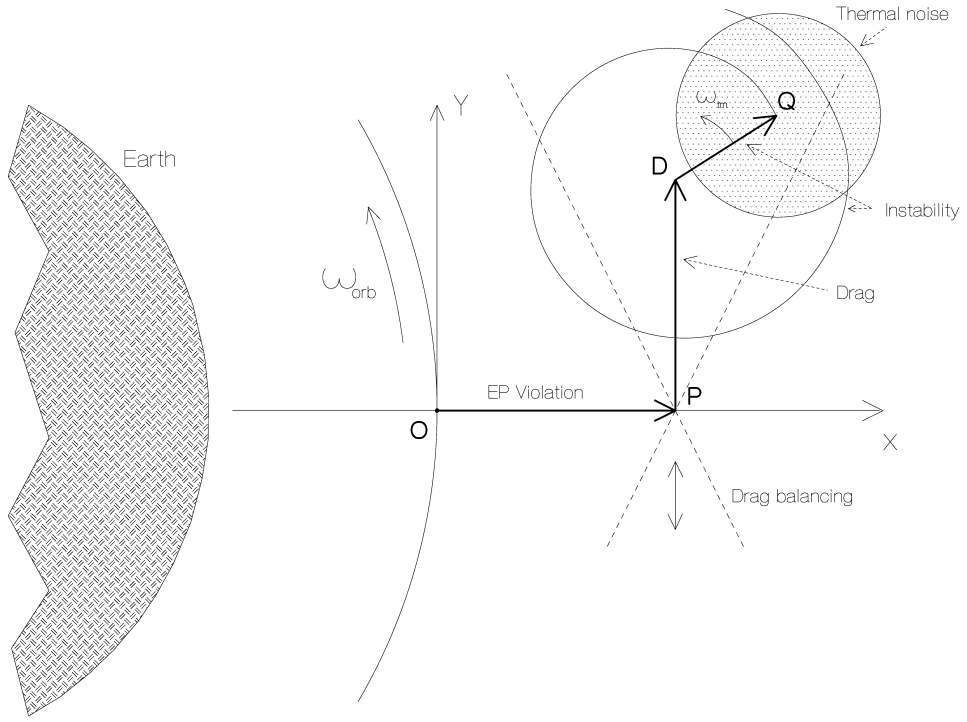

Fig. 11. Qualitative representation, in the orbital plane and for one pair of test masses, of the differential displacements obtained from the synchronous demodulation of the 2-phase 5 Hz signal. The *x*-axis is in the Earth-to-satellite direction and the vector *OP* is the differential displacement, directed along the *x*-axis and constant in amplitude, of the two masses due to an EP violation. The perturbation *PD* due to the initially unbalanced atmospheric drag will be found in the area between the two dotted lines crossing in *P*: the angle between them is about 0.8 rad, and is due to the fact that the drag has a variable component in the radial direction because of the solar radiation pressure (of amplitude about 0.4 times the atmospheric drag and in the Sun–satellite direction). Smaller contributions to the *PD* vector come from the Earth albedo, the Earth infrared radiation and, by a smaller amount, from a possible small eccentricity of the orbit. By finely adjusting the lengths of the suspension arms the point *D* is displaced up or down inside this area, and this balancing of the drag should be continued until *D* is as close as possible to *P*. In doing so, also the radial component is automatically balanced. The resonant variations of the drag (not shown) will oscillate inside the same area. The vector *DQ* is the instability due to the internal dissipation of the springs (Section 3.2), slowly rotating and increasing: it must be actively damped until *Q* is as close as possible to *D* (and *P*). The circle around point *Q* represents the error in the measurement due to the thermal noise of the mechanical oscillations in a few days of integration time. The actual values of all these quantities are discussed in the text.

1%. With an absolute drift of 10^{-9} per day, it would take 100 days before springs originally equal were to differ by 1 part in 10^7.

It is apparent that the capability to reject the common mode effect of inertial forces on the test masses is crucial for the EP experiment. Let us therefore consider the problem of manufacturing equal suspension springs for the test masses inside each chamber. A level $\Delta k/k \simeq 10^{-3}$ can be achieved by construction on Earth with computer controlled precision techniques. Once the springs have been properly built (carved, annealed, etc.) the problem arises to check their properties, in order to establish to which extent they equal each other, and to measure the level of flicker noise. It is apparent that hair-like springs such as these cannot be loaded on Earth with the masses they are supposed to suspend in space, and a scaled model would not be of great

value. It has been suggested by V.B. Braginsky (Braginsky, 1993) to use appropriate torsion balances such that motion in the horizontal plane is dominated by the elastic constant of the springs; by mounting the springs as in Fig. 12, and using optical measurement techniques it is possible to measure how equal are the elastic constants, the amount of their variation with time and the level of flicker noise.

We therefore assume a common mode rejection, by construction, of 10^{-3} and plan to achieve the required level of 10^{-7} during a calibration phase at the beginning of the mission in which any 5 Hz signal detected by the read out system is reduced down to the expected signal. In order to make this possible a coupled suspension of the test masses is proposed (see Fig. 2). The masses are attached by means of soft springs to the ends of two rods, and each rod is pivoted at its middle point on elastic gimbals so that it can change orientation by small amounts in all directions. In this way the frequency of oscillations in common mode depends on the elastic constant k of the suspension springs, while the frequency of oscillations in differential mode (i.e. of one mass with respect to the other) depends on k_{tor}/l^2, where k_{tor} is the elastic constant of the torsion wires of the gimbals and l is the length of each of the four halves of the two rods connecting the gimbals to the springs. Thus, by adjusting the length of the rods it is possible to balance the effect of forces which are inherently common mode but nonetheless give a differential effect because of small differences in the elastic constant of the suspensions. Were the masses suspended independently (i.e. springs attached directly to PGB laboratory without gimbals) the only way to balance the effect of perturbations in common mode would be by in flight changes of the elastic constant of the springs itself, which would be very hard to achieve and control.

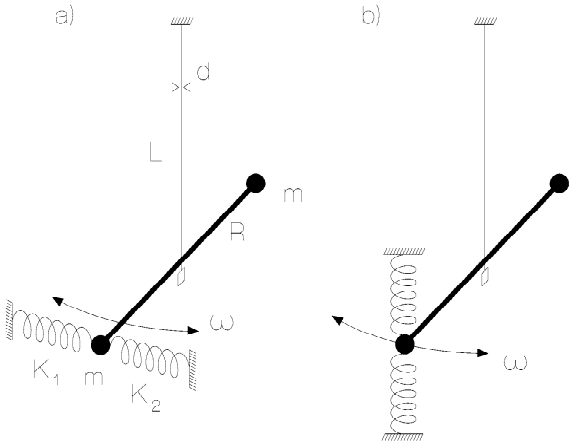

Fig. 12. Testing of suspension springs. By means of a torsion pendulum one can make ground tests of the longitudinal (a) and of the transversal (b) characteristics of the very thin and weak springs that will be used in orbit at zero g. One can test one spring at a time or, as shown in this figure, measure the differences between two of them.

Fig. 13 shows an enlargement of the elastic gimbals and the piezoelectric actuators, with the polarization and the applied constant voltages whose sum and difference allow us to adjust the axial position of the barycentres (Section 4) and to displace the centres of mass of the four halves of the two rods. In this way it is possible to compensate for any remaining differences in the suspensions that would otherwise produce differential motions of the test bodies under the effect of inertial and tidal forces, the driving signal for these adjustments being the (demodulated) 5 Hz signal itself. To the achieved level of balance, no inertial force – no matter how variable – will produce any relative displacement of the test masses. The system is conceptually similar to an ordinary balance on the ground. Considering that sensitive balances on the ground, at 1 g, can detect changes of weight of 10^{-7}–10^{-8} (Quinn, 1993), and given the extremely good properties of piezoceramics for fine adjustments, a similar common mode rejection factor can be achieved with this system at almost zero g. Once no further reduction is possible the phase and frequency of the signal must be analysed in order to establish whether it is due to an EP violation. How can one be sure that an EP violation signal is not eliminated together with the perturbing effects? This would only be possible for a competing effect with the same frequency and phase as the signal in the case that it were also constant in

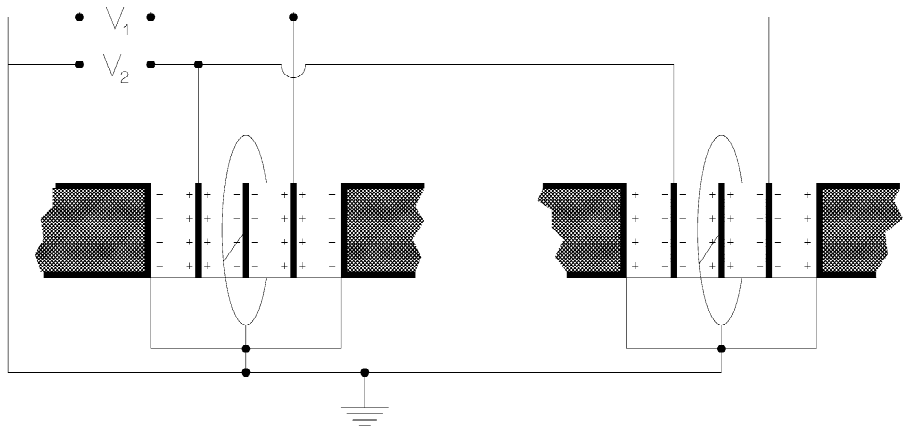

Fig. 13. The system of piezoelectric actuators placed in the two balancing rods. The + and − signs represent the intrinsic polarization of the actuators, i.e. how each one of them must be oriented when mounted. Control voltages are applied to the actuators (when they are applied with the opposite polarity they should not exceed a certain value, which however is relatively high, so as not to risk to depolarize the piezoelectrics): the sum $V_1 + V_2$ determines the relative axial position of the barycentres of the test masses and is used for axial centering (Section 4). The voltage difference $V_1 - V_2$ can be used to change the lengths of the four halves of the rods so as to balance out the effect of transverse inertial forces (in particular the along-track component of the air drag).

time. If the effects of drag and EP violation were parallel to each other one could, for one particular value of the drag, balance the sum of the two; but drag is variable, and therefore balancing would not hold. Furthermore, the two effects are in fact about 90° apart. Once the largest common mode effect has been balanced it means that – to this level – the suspensions respond the same, therefore also balancing all other common mode effects. Later checks of the observed (if any) 5 Hz signal should be performed to make sure that there has been no long term variation of the suspensions which may require to repeat the initial adjustment procedure.

Other experiments which require a good rejection of common mode effects are worth considering in order to compare the different levels of CMR. Let us first consider STEP, which is the closest experiment to GG and plans to reach a CMR factor of 10^{-5} (Worden et al., 1990; Barlier et al., 1991; Blaser et al., 1993, 1994, 1996). There is a major difference between STEP and GG. The STEP configuration is unfavourable because a displacement signal about 10 orders of magnitude smaller than the length of the symmetry axes of the test masses is expected to take place just along the common direction of these axes, which obviously means that any transversal perturbation in common mode can generate the same type of signal if the two axes are not sufficiently well aligned. The CMR goal of STEP is limited precisely by the capability to align the axes of the two accelerometers on one another. This is not so in GG, where the signal acts in the plane perpendicular to the spin/symmetry axes of the cylinders and common mode forces can be rejected very effectively like in sensitive balances on the ground. Instead, STEP relies on drag-free technology to partially compensate for the drag, which necessarily means relying on the technology of mechanically tuned Helium thrusters. More advanced thrusters under development in Europe have been proposed for STEP (Blaser et al., 1994), namely FEEP, which have the advantages of very high specific impulse, very fine electrical (rather than mechanical) tuning and negligible mass of propellant (liquid Cs). However, since a large quantity of He propellant must be carried on board of STEP anyway (in order to make the experiment cryogenic) and the boiled off He must in any case be eliminated in a carefully

controlled manner in order not to disturb the experiment, it seems reasonable to use the boiled off He as propellant for the drag compensation system, as originally proposed by Worden and Everitt. The use of FEEP proposed by Blaser et al. (1994) for STEP was instrumental to the competition within ESA and was soon proved not viable (Blaser et al., 1996).

Gravity gradiometers, which have reached a CMR level of 10^{-5} (Park, 1990), may appear as possessing similarities with GG. As a matter of fact this is not the case because they use separate and uncoupled accelerometers. To the contrary, in GG the test masses are not separate but mechanically coupled: even though they are concentric and very accurately aligned, the dynamics of their motion is similar to that of balances and torsion balances (see Fig. 12b where the wire is used only for suspending and as an axis of rotation, without torsion) because they are suspended on the opposite ends of two arms pivoted at their centres, as in balances and torsion balances. The capability to reject common mode effects depends, in GG, on two facts: (a) the stability of springs (both in time and with temperature); (b) the characteristics of the piezoelectric actuators to be used for in flight adjustments of the length of the arms. None of these crucial issues is of any concern for researchers on gravity gradiometers or on STEP; hence there is no reason why the CMR factor of the GG apparatus should have any relation to the CMR factor of these apparata. To the contrary, the issue of springs stability is typically of great interest for scientists who build and use room temperature gravimeters for accurate measurements of Earth tides, since spring gravimeters use similar (metallic) springs and face very similar stability problems.

5.3. Low frequency effects

Although the largest effect of air drag is at the orbital frequency of the satellite, other low frequency variations (in the range from the orbital frequency to near the threshold frequency of the PGB laboratory) which are too low to be damped by the mechanical suspension, cannot be ruled out. They act on the test bodies as inertial forces of which only the differential effect does matter as far as detecting an EP violation is concerned; if a total CMR factor of 10^7 is achieved, their common mode effect is also reduced by this factor. Furthermore, while the inertial force resulting from the main along-track component of the drag is seen by the capacitance sensors at exactly the same frequency as an EP violation signal (the direction of the acceleration due to air drag changes at the orbital frequency just like the satellite-to-Earth direction of an EP violation), a higher frequency variation of the drag is seen by the sensors at a frequency differing from their spinning frequency with respect to the centre of the Earth (i.e. the frequency of an EP violation) by an amount which is given by the frequency of that particular air drag variation (Fig. 11). Therefore, besides being reduced by common mode rejection these effects can be distinguished by measuring the rotation rate of the spacecraft with ordinary star trackers or Earth elevation sensors. After the demodulation of the signal at 5 Hz (Fig. 11) they appear as very regular oscillations (due to the high Q; see Section 6.2)) at about 90° with respect to a constant signal, and are therefore easily distinguishable. By taking the average value of two measurements at a time interval of half their period we can determine the centre of the oscillations with an error $\lesssim 1/\sqrt{(2Q)}$, which is certainly better than we need.

The GG coupled test bodies have low natural frequencies of oscillation both in common mode and in differential mode (see Section 3.2). There will be air drag disturbances at these frequencies due to air density variations (*"air granularities"*) over distance scales of about a thousand km. The corresponding density is smaller than average atmospheric density, typically by at least a factor of 10. For these disturbances to resonate with the natural frequencies of the system, they must act at a frequency whose distance from the resonant frequency $\omega_{\rm res}$ is within the width of the gaussian, namely $\omega_{\rm res}/Q$. With $Q \simeq 19\,000$ for the test bodies of the GG experiment (see Section 6.2) there is no way that air granularities over a thousand km can act on the spacecraft so precisely close to the natural frequencies of the test bodies.

We conclude this section on inertial forces by saying that this version of GG is designed in such way that EP testing is possible without eliminating the common mode effect of air drag. Its differential effect on the test masses is transformed by the mechanical suspension in a difference of inertial forces that can therefore be adequately reduced, partly by construction in the ground laboratory, partly by small and fine in flight adjustments at the beginning of the mission. It might be necessary to repeat the calibration, but only a few times during the $\simeq 6$ months duration of the mission. Such adjustments of differential effects are much smaller and less demanding than it would be to counteract the effect of air drag itself on the spacecraft. Indeed, beside being required only once (or a few times), they are extremely fine for them to be realized with piezoceramics, whose precision and reliability as actuators are well known, thus avoiding any thruster firing.

6. Room temperature effects

It is well known that a small force gravitational experiment in space should avoid the presence of nearby moving masses. Therefore, were a refrigerating material carried on board the spacecraft – close to the apparatus – in order to lower the temperature, it should be accurately confined, which is neither easy nor inexpensive. We choose to operate the experiment at room temperature and find that, because of the (relatively) high spin rate of the spacecraft and the intrinsic differential nature of the signal, it is possible to obtain an adequate level of temperature stability by passive thermal isolation only (Section 6.1). As for thermal noise, we use bigger test masses than STEP in order to compensate for the fact of operating at higher temperature (Section 6.2). A capacitance read out system which exploits the differential nature of the experiment can provide an adequate measurement accuracy (Section 7) with no need to resort to a low temperature measurement device.

6.1. Temperature stability

For the reasons discussed in Section 2.2 a 520 km altitude, almost equatorial, almost circular orbit is the best choice for the experiment. However, on this orbit the satellite spends almost half of its time in the shadow of the Earth and the rest in sunlight, thermal equilibrium temperatures in the two cases differing by several tens of degree. While azimuthal temperature variations are inexistent because of the the fast spin, temperature gradients between the illuminated and the dark side of the satellite when exposed to radiation can in principle be very large. These gradients can be essentially eliminated inside a rapidly spinning spacecraft if it is properly insulated. Insulation and vacuum serve also the purpose of reducing the rate of temperature variation with time. Temperature stability in time inside the PGB laboratory should be of 0.01 K for the required integration time of about 2.6 hours (Section 6.2), but possibly longer.

Vacuum is needed also not to reintroduce acoustical noise on the PGB laboratory and the test masses. The vacuum level that can be achieved by means of a hole to open space is that corresponding to atmospheric density. At 520 km altitude (where atmosphere is mostly constituted by molecular oxygen) $\rho_{\rm atm} \simeq 2.04 \cdot 10^{-16}\,{\rm g\,cm^{-3}}$, hence $p_{\rm atm} \simeq 1.7 \cdot 10^{-10}$ torr. In fact the pressure may be about a factor 10^3 bigger because of outgassing. However, care should be taken in avoiding materials with high levels of outgassing and in setting the size of the holes on the basis of the outgassing area. Experience with resonant bar antennas for the detection of gravitational waves shows that gold coated Kapton should be used instead of Mylar because of its lower outgassing level. Any anisotropy in the internal outgassing (from some particular spots) rotates with the test bodies and the sensors. It therefore gives an essentially DC effect.

The heat sources that the satellite is exposed to are the Sun ($\Phi_\odot \simeq 1.4 \cdot 10^6\,{\rm erg\,s^{-1}\,cm^{-2}}$ at the Earth's distance) and the Earth itself, in the visible as well as in the infrared range. The Earth emits a fraction of the sunlight given by its albedo (0.3 on average,

although widely variable) i.e. $\Phi_{\oplus} \simeq 0.3\Phi_{\odot}$. In the infrared, at the surface, we have $\Phi_{\oplus}^{\mathrm{IR}} \simeq 2.4 \cdot 10^5\,\mathrm{erg\,s^{-1}\,cm^{-2}}$. A source of heat from a given direction will produce a temperature gradient across the satellite between the side facing the source and the one away from it, and eventually a gradient across the test bodies and the suspended springs. A temperature gradient across the test bodies is a source of radiation pressure, and since the satellite is spinning, the resulting signal is modulated at the spinning frequency (as measured with respect to the source of heat). The spinning frequency with respect to the Earth, namely the source of an EP driving signal, is not the same as the one with respect to the Sun, and they can be distinguished from one another. However, possible temperature gradients due to the infrared radiation from the Earth would have exactly the same signature as the EP violation we are testing. We must therefore make sure that internal temperature gradients be adequately small. Indeed, we can see that temperature gradients across a rapidly spinning spacecraft can be reduced by many orders of magnitude by means of an insulating outer shell and the vacuum inside.

A cylindrical shell spinning with period P and exposed to the solar flux $\Phi_{\odot}$ (e.g. perpendicular to the spin axis) will have a temperature gradient $\Delta\Theta = (\Phi_{\odot} P \alpha_{\mathrm{ab}})/(\pi\rho c_{\mathrm{sh}} w)$ where ρ is the density of the shell, α_{ab} its absorption coefficient (absorbed to impinging flux), w its thickness and c_{sh} its specific heat. For a spin period $P \simeq 0.2\,\mathrm{s}$ and $w \simeq 1\,\mathrm{cm}$ the typical value of $\Delta\Theta$ is around $1/200$ degree for a good insulator (e.g. glass) and $1/400$ for a good heat conductor (e.g. Copper). However, if the spin period of the shell is much smaller than the timescale of its thermal inertia, it is as if it were subject to an isotropic flux, hence resulting in a negligible gradient.

Let the inner surface of the spacecraft cylindrical body be covered with an insulating shell; the temperature behaviour across the shell will be given by:

$$T(x) = T_{\circ} + (T_E - T_{\circ})e^{-x/d} \tag{29}$$

where $T_{\circ}$ is the satellite initial temperature (when injected into its orbit), T_E is the temperature of external environment and d is the penetration depth. Since the spacecraft spins fast we can assume that T_E is the same all over its surface. We have:

$$d \simeq \pi\sqrt{\frac{Pk_{\mathrm{tc}}}{2\rho c_{\mathrm{sh}}}} \tag{30}$$

where ρ, c_{sh} and k_{tc} are the density, specific heat and thermal conductivity of the insulating shell. Taking for these quantities typical values for Kapton or Mylar (as given by DUPONT or found by Immergut, 1984) we get $d \simeq 0.03\,\mathrm{cm}$. If the insulating shell has a thickness of 1 cm, it is apparent from Eq. (29) that gradients of temperature in the plane perpendicular to the symmetry axis are negligible. As for the top and bottom sides of the cylindrical spacecraft, they can be coated with reflecting material (mirrors) in order to reduce solar heating, since it would be differential. This technique is widely used, e.g., in geosynchronous satellites. In addition, it is worth recalling a very important peculiarity of the GG experiment, namely that the spacecraft is connected to the experimental laboratory only through the hair-like suspension springs of the PGB laboratory (inside which the requirement on thermal stability must be achieved) and that there is vacuum inside the spacecraft. Hence, heat is transferred essentially by radiation (see below). Temperature gradients along the symmetry axis modulated at the orbital frequency would give an effect at the spin/signal frequency. Let us consider the effect of axial gradients on the arms. A differential expansion of the arms in the coupled suspension of the test masses would destroy the balancing and therefore reduce the capability to maintain the required CMR factor of 10^{-7} discussed in Section 5.2. We therefore need:

$$\frac{\Delta l}{l_{\circ}} \lesssim 10^{-7} \tag{31}$$

If α is the expansion coefficient of the arms and z the axial coordinate:

$$\frac{\Delta l}{l_{\circ}} \simeq \alpha \cdot \left(\frac{\Delta T}{\Delta z} \cdot l_{\circ}\right) \tag{32}$$

Since materials with $\alpha = 10^{-5}\,\mathrm{K}^{-1}$ are common and can be used for manufacturing the arms, it follows that axial temperature gradients over the arm's length (a few cm) must be smaller than 0.01 K, which is not a stringent requirement. Were it needed, one could make the arms of a material with $\alpha = 10^{-6}\,\mathrm{K}^{-1}$, thus allowing for gradients of 0.1 K.

The average temperature of the spacecraft changes because of it going in and out of the Earth shadow, i.e. the relevant frequency is the orbital one. In order to keep the temperature stable with time we must reduce the incoming heat. Since the cylindrical surface of the spacecraft must be covered with solar cells (in order to generate the necessary electric power) the external surface will absorb most of the heat and reach, more or less, equilibrium with the solar radiation. Hence, we need – on the internal side of the spacecraft – an insulating shell in order to reduce the amount of heat that will reach the interior of the satellite. The timescale τ of thermal inertia provided by an insulating shell of thickness w is:

$$\tau = \frac{\rho c_{\mathrm{sh}}}{k_{\mathrm{tc}}} \cdot w^2 \tag{33}$$

with ρ, c_{sh} and k_{tc} the density, specific heat and thermal conductivity of the insulating material. Then, the time variation of the temperature at the internal surface of the insulating shell is:

$$T(t) = T_E + (T_\circ - T_e) \cdot e^{-t/\tau} \tag{34}$$

(T_E and $T_\circ$ as defined above). Let us consider one half satellite orbit in sunlight. At the end of half period in sunlight the temperature of the internal surface of the insulating shell will be:

$$T_{\mathrm{sh}}(P_{\mathrm{orb}}/2) \simeq T_{E_s} + (T_\circ - T_{E_s}) \cdot \left(1 - \frac{P_{\mathrm{orb}}}{2\tau}\right) \tag{35}$$

where T_{E_s} is the equilibrium temperature in sunlight. Using $w \simeq 2.5$ cm and the properties of materials like Kapton and Mylar we have $\tau \simeq 6.2 \cdot 10^3$ s, while $P_{\mathrm{orb}}/2 \simeq 2850$ s. The corresponding temperature variation (after half period in sunlight) is:

$$(\Delta T_{P_{\mathrm{orb}}/2})_s \simeq \frac{P_{\mathrm{orb}}}{2\tau} \cdot (T_{E_s} - T_\circ) \tag{36}$$

Similarly, the temperature variation after half period in the shadow of the Earth (darkness) is:

$$(\Delta T_{P_{\mathrm{orb}}/2})_d \simeq -\frac{P_{\mathrm{orb}}}{2\tau} \cdot (T_{E_d} - T_\circ) \tag{37}$$

where T_{E_d} is the equilibrium temperature of the satellite when in the dark. Let us consider a large difference of 50 K between equilibrium temperatures in sunlight and in darkness (when the satellite is exposed only to the infrared radiation form the Earth), and a satellite initial temperature halfway between the two. Then, the temperature variation on the internal side of the insulating shell after half orbit period will be (in absolute value) $\Delta T_{P_{\mathrm{orb}}/2} \simeq 11$ K. Obviously the two temperature variations (increase when in sunlight and decrease when in darkness) will not cancel out. Let us take half of each. This means that, after one full orbital period of the satellite around the Earth the temperature on the internal side of the insulating shell is changed by:

$$\Delta T_{P_{\mathrm{orb}}} \simeq 6\,\mathrm{K} \tag{38}$$

This is too much for our requirements. We now exploit the important fact of having good vacuum inside the spacecraft, because it ensures that there is only radiative transfer of heat (apart for the thin hair-like suspension springs of the PGB laboratory). Indeed, the mean free path of gas molecules at room temperature and 10^{-4} torr is about 1 m, while we have about $1.7 \cdot 10^{-7}$ torr (having allowed a factor 10^3 for outgassing). We can also coat the external surface of the PGB with Kapton. Then, the amount of energy transferred from the insulating shell to the Kapton coated external surface of the PGB after 1 orbital period is:

$$E_{P_{\mathrm{orb}}} = \sigma T_\circ^3 \Delta T_{P_{\mathrm{orb}}} \epsilon_k A P_{\mathrm{orb}} \tag{39}$$

where σ is the Stefan-Boltzmann constant, ϵ_k is the emissivity of kapton and A the area of the surface involved ($A \simeq 1.13 \cdot 10^4\,\mathrm{cm}^2$). The corresponding temperature variation of the PGB laboratory (made of Copper) is:

$$(\Delta T_{\rm PGB})_{P_{\rm orb}} = \frac{E_{P_{\rm orb}}}{c_{\rm Cu} M_{\rm PGB}} \quad (40)$$

where $c_{\rm Cu}$ is the specific heat of Copper and $M_{\rm PGB}$ is the mass of the PGB laboratory. We get $(\Delta T_{\rm PGB})_{P_{\rm orb}} \simeq 3.4 \cdot 10^{-3}$ K. After 5 days, i.e. about 76 orbits of the satellite we shall have:

$$(\Delta T_{\rm PGB})_{5\ \rm days} \simeq 2.6 \cdot 10^{-1}\ {\rm K} \quad (41)$$

Multilayers of insulating material are usually used in cryogenic experiments (Haselden, 1971), because, if properly separated in order to reduce heat conduction, they are known to provide a reduction of the transferred power proportional to the number of layers employed. For instance, this technique is successfully used to reduce the amount of input power on the very large cryostats which enclose resonant bars ($\simeq 2$ ton) for low temperature detection of gravitational waves (the EXPLORER antenna at CERN, in Geneva, and the NAUTILUS antenna in Frascati, Rome). Our problem is easier because of both the smaller size of the device and the very tiny connection between the spacecraft and PGB. In any case, from Eq. (41) it follows that a number of about 30 Kapton layers (such as those commercially available from DUPONT, of $\simeq 50\ \mu$m thickness each) can provide the required level of thermal stability.

As far as internal power sources are concerned, we recall that they will be rotating together with the entire system, so all resulting effects will be DC. We shall also take care to use low dissipation components. In addition, only the preamplifiers will be positioned on the supporting rod inside the hollow cylinder test bodies; all the remaining power sources will be placed on the internal surface of the spacecraft shell. The required number of wires can be accommodated either as independent helicoidal springs or by grouping them on a plastic support without any serious problem of degrading the reduction of vibrational noise since a low Q is required for the PGB suspensions. Most of the wires will go to the inch-worms, to the active dampers, to the locking-unlocking mechanisms and to the preamplifiers of the capacitance read out while only 4 wires go through the gimbals to the piezoceramics on the balancing arms (see Fig. 2). For the passage through the multilayer insulation on the outer side of the PGB laboratory we can use, if needed, a technique known as *thermal sink*, whereby the wire does not go straight inside but rather makes many turns so as to largely reduce the temperature gradient that it will bring in. This technique is currently employed in the EXPLORER and NAUTILUS cryogenic resonant bar antennas mentioned above.

LISA (Laser Interferometer Space Antenna) (Bender et al., 1994), a proposed space mission for the detection of gravity waves, is another example of a noncryogenic space experiment where a very good thermal stability is needed, to be achieved passively. For LISA the requirement is of $10^{-6}\ {\rm K}/\sqrt{\rm Hz}$ around 1 mHz. LISA has the advantage, over GG, to be subject to a much smaller variation of the solar flux due to its heliocentric orbit. However, GG has the advantage, over LISA, of spinning fast (while LISA is space stabilized). In the ground torsion balance Eöt-Wash experiment (Su et al., 1994) (also noncryogenic) they use two active temperature stabilization systems based on several temperature sensors in order to achieve a stability of 0.02 K across the experimental chamber. We recall that their balance rotates very slowly, with a period of 6231.2 s, while the spin period of GG is only 0.2 s.

Residual gas particles inside the spacecraft accelerated by a temperature gradient between two sides of a test body would result in an acceleration necessarily different for the two bodies: $a_{\rm re} = p(\Delta T/\Delta x)/(2\rho_{\rm tm} T)$ with $\rho_{\rm tm}$ the density of the test mass. This is the radiometer effect that the STEP experiment is concerned about. The reason why this is so is that in STEP the signal is along the symmetry axis of the test cylinders; for a given residual gas pressure any temperature gradient between the two bases of each cylinder will result in an acceleration along its symmetry axis, and it would inevitably be a differential acceleration; if temperature variations are modulated at orbital frequency this would mimic an EP violation. In STEP this problem is solved by having an extremely low residual gas pressure (as low as 10^{-13} torr, made possible by very low temperature)

and a requirement for temperature gradients across each test body not to exceed $\simeq 1\,\mathrm{mK}$. In the GG design this effect is of no concern because the signal is normal to the symmetry axis of each cylinder, hence if its inner and outer surface are at different temperatures, the net force by thermally accelerated residual gas would be zero for symmetry reasons. Only if temperature dos not have azimuthal symmetry there can be a radiometer effect; which is not the case because of fast spin.

The effect of viscous drag due to the residual gas on the centre of mass of the sensing bodies is well below the signal even under conservative assumptions. The effect is estimated according to Milani et al. (1987), Ch. 6, taking into account that the thermal velocity of the gas molecules is much higher than the velocity of the test bodies.

We must not forget that solar cells will necessarily cover the outer surface of the spinning spacecraft whose temperature gradient can be as large as $1/200$ of a degree. It is only after an appropriate insulating shell that this gradient is significantly reduced. Therefore we must expect that the outermost layer of the spacecraft (essentially the solar cells) will be subject to nonuniform thermal expansion at the spinning frequency. However, since the part of the spacecraft involved in this oscillation is only the external one (because temperature gradients are negligible inside) the result is a forced term acting on the suspension at frequency ω, which will be reduced according to the transfer function of Fig. 3, and the effect can be neglected. We must also expect that the outermost layer of the spacecraft will be subject to nonuniform thermal expansion at the orbit frequency, resulting in a common mode oscillation of the test masses at that frequency similar to the effect produced by the along track component of air drag. With a typical expansion coefficient $\alpha \simeq 10^{-5}\,\mathrm{K}^{-1}$ and a temperature gradient which, thanks to the rapid spin, is not larger than about $1/100\,\mathrm{K}$, the oscillation amplitude of the outer shell will be of a few $10^{-6}\,\mathrm{cm}$. A common mode rejection of 10^{-5} is enough to make this effect smaller than the signal (Section 5.2). As for the corresponding gravitational effects, they are found to be negligible. The expansion/contraction of the outer shell of the spacecraft (due to it entering and exiting the shadow of the Earth), the resulting changes in moment of inertia and spin rate, and how to compensate for them are discussed in GALILEO GALILEI (1996) (Ch. 2.1).

We now investigate the effects of thermal expansion of the test bodies. Let us first consider the simpler case in which the test bodies expand uniformly. They will have expansion coefficients of the order of $\simeq 10^{-5}\,\mathrm{K}^{-1}$, because their composition is selected on the basis of EP violation considerations and obviously not with the purpose of minimizing their thermal expansion. Furthermore, their expansion coefficients will not be the same, and indeed we shall assume that they differ by its entire value, namely that there is a difference in their expansions by $\simeq 10^{-5}\,\mathrm{K}^{-1}$ too. However, as long as they expand *uniformly*, there is *no relative displacement* of their centres of mass and therefore no differential effect on the read out capacitors.

But test bodies will not be perfect, and in correspondence of inhomogeneities in their mass distribution there might be a different response to temperature variations. However, the direction of non uniform expansion being fixed with the test body it is also fixed with respect to the sensors, which means that its effect is DC and does not compete with an EP violation signal. Furthermore, it is also small because of it being proportional to inhomogeneities of the test bodies. With a not too stringent requirement on the mass density such as $\Delta\rho/\rho \simeq 10^{-3}$, and in the conservative assumption that mass inhomogeneities do necessarily imply a nonuniform thermal expansion of the same level (i.e. with a proportionality factor of 1), we get a relative motion of the centres of mass by about 10^{-10}, which means (for linear dimensions of about 10 cm) differential displacements in the direction of the mass inhomogeneity by $10^{-9}\,\mathrm{cm}$, which is perfectly satisfactory for a DC signal.

We must also consider the fact that a uniform (but different) expansion of the test bodies will change the distances a and b of the capacitors from the outer and inner surfaces – respectively – of the test bodies (Section 7). We shall see in Section 7 that in order to

be sensitive to an EP violation of $\eta = 10^{-16}$ the read out capacitance plates must be centered between the test masses to within $\simeq 20$ Å which, in relative terms means $\simeq 4 \cdot 10^{-7}$. Active balancing to this level is done with inch-worm actuators (see Section 7) and can be repeated if necessary. A difference in the expansion coefficients by $\simeq 10^{-5}\,\mathrm{K}^{-1}$ and a thermal stability of 0.01 K allow us to maintain this level of balancing. However, were it necessary, there is a possibility to reduce the differential displacement of the surfaces of the test bodies with respect to the capacitance plates in between. We can build the frame which supports the capacitors (see Fig. 2) using an appropriate alloy whose expansion coefficient must be such to compensate for the differential expansion of the test bodies. Once the material choice for the EP experiment has been made and the test bodies have been built their radii and thermal expansion coefficients can be accurately measured, thus uniquely determining the required value for the expansion coefficient of the frame. In this way it is possible to reduce the differential expansion by about a factor of 10, thus reducing the relative displacement.

Finally, temperature variations will affect the stiffness of the suspension springs and therefore change the value of the transversal elongation Δx in response to the inertial force caused by air drag acting on the spacecraft:

$$\frac{d\Delta x}{dT} = -\frac{m a_i^{\mathrm{c.m.}}}{k^2(T)} \cdot \frac{dk(T)}{dT} \tag{42}$$

We must have:

$$\frac{d(\Delta x)}{m a_i^{\mathrm{c.m.}}/k(T)} = -\left(\frac{1}{k}\frac{dk(T)}{dT}\right) \cdot dT \lesssim 10^{-7} \tag{43}$$

since 10^{-7} is the required level of CMR. With a maximum temperature change of 0.01 K and $1/k \cdot (\Delta k/\Delta T) \simeq 10^{-6}\,\mathrm{K}^{-1}$ as obtained in gravimeter springs (see Section 3.2) the effect is 10 times smaller than it is needed, thus allowing for a less good thermal stability of the springs.

All the above analysis of the perturbing effects to be expected in performing the experiment at room temperature is based on simple physical principles; a more detailed thermal analysis has been conducted in GALILEO GALILEI (1996) taking advantage of space industry experience on the subject.

6.2. Thermal noise and integration time

Test masses will have their own mechanical thermal noise, resulting in a perturbing thermal acceleration on the test mass $a_{\mathrm{th}}^{\mathrm{tm}}$ that must be smaller than the signal acceleration $a_{\mathrm{EP}} \simeq 8.4 \cdot 10^{-14}\,\mathrm{cm\,s^{-2}}$. At room temperature $T \simeq 300\,\mathrm{K}$ we have:

$$\frac{a_{\mathrm{th}}^{\mathrm{tm}}}{\sqrt{\mathrm{Hz}}} \simeq \sqrt{\frac{4K_B T \omega_{\mathrm{tm}}^{\mathrm{d.m.}}}{mQ}} \tag{44}$$

and

$$a_{\mathrm{th}}^{\mathrm{tm}} \simeq \sqrt{\frac{4K_B T \omega_{\mathrm{tm}}^{\mathrm{d.m.}}}{mQ}} \cdot \frac{1}{\sqrt{T_{\mathrm{int}}}} \tag{45}$$

where K_B is the Boltzmann constant, $m \simeq 10\,\mathrm{kg}$ is the mass of each test body, $\omega_{\mathrm{tm}}^{\mathrm{d.m.}} \simeq 2 \cdot 10^{-2}\,\mathrm{rad\,s^{-1}}$ their natural frequency for differential oscillations, Q the mechanical quality factor and T_{int} the integration time.

If we take the $Q \simeq 500$ value, as used in the numerical simulation of Section 3.2, we get $a_{\mathrm{th}}^{\mathrm{tm}}/\sqrt{\mathrm{Hz}} \simeq 2.57 \cdot 10^{-11}\,\mathrm{cm\,s^{-2}}/\sqrt{\mathrm{Hz}}$, which means that an integration time of about 4.35 days is necessary in order to reach a signal-to-noise ratio of 2. However, we have now manufactured helicoidal springs similar to the ones to be used in the space experiment to suspend the test masses GG (GALILEO GALILEI, 1996). By setting the spring in horizontal oscillation (for the oscillations not to be affected by local gravity) with vacuum, temperature and clamping similar to those expected in the space experiment, and at the same frequency at which it will spin – hence undergo deformations – in space, we could measure the mechanical quality factor getting a value of 19 000. Since losses due to the electrostatic dampers are much smaller (Section 3.2) and all other parts are rigid with no expected dissipation, this result gives a realistic value for the total mechanical losses (further improvement may be possible). Using

$Q \simeq 19\,000$ in Eq. (45) we get $a_{\rm th}^{\rm tm}/\sqrt{\rm Hz} \simeq 4.07 \cdot 10^{-12}\,{\rm cm\,s^{-2}}/\sqrt{\rm Hz}$ and an integration time of about 2.6 hours for a signal-to-noise ratio of 2 as before.

Note that in Eqs. (44) and (45) we have the natural frequency of oscillation of one test body with respect to the other instead of the (higher) natural frequency of oscillations in common mode ($\omega_{\rm tm}^{\rm c.m.} \simeq 3.95 \cdot 10^{-2}\,{\rm rad\,s^{-1}}$). This is correct because, since the two frequencies are not close (they differ by about a factor of 2) and Q is high, the bandwidth of noise is so small that there is no significant contribution from the thermal noise in common mode to the thermal noise in differential motion where the effect of an EP violation would appear. It is also worth noticing that the perturbing effect of thermal noise is proportional to $(T/m)^{1/2}$, which explains why – working at room temperature – it is important to have test bodies of relatively large mass. In comparison with STEP we work at 100 times higher temperature and therefore use test bodies about 100 times more massive. As for the thermal noise perturbation due to the PGB laboratory, i.e. the common mode thermal noise of the platform, it is given by formulas similar to Eqs. (44) and (45) with the natural frequency, mass and quality factor of the PGB laboratory (higher mass, lower Q). Being a small common mode effect it is easily rejected.

7. The capacitance read out system

The displacements of the test masses are detected with a pair of capacitors in a circuit which is essentially an LC bridge, formed by two resonant coupled oscillators, as shown in Fig. 14. The plates of the capacitors are sections of cylinders concentric to the test bodies (Fig. 15) and are supported by the frame shown in Fig. 2.

A voltage signal $V_{\rm in}$ of angular frequency $\omega_{\rm in}$ is applied to the bridge in order to shift the signal of interest to a frequency band with a $1/f$ noise as small as possible. We consider $\nu_{\rm in} = \omega_{\rm in}/(2\pi) \simeq 1\,{\rm MHz}$. The circuit has the greatest sensitivity when $L = (1/C_1 + 1/C_2)/\omega_{\rm in}^2$ and when also the output circuit resonates at the same frequency ($\omega_{\rm out} = \omega_{\rm in}$). Since

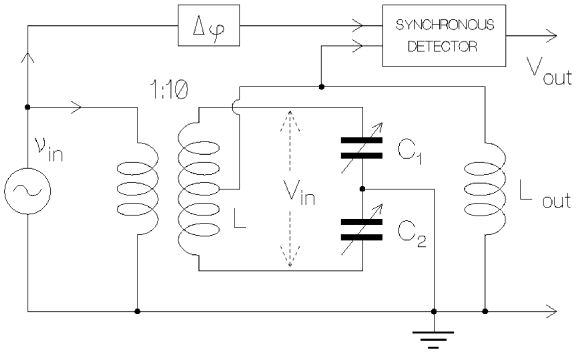

Fig. 14. Outline of the read-out circuit. The two variable capacitors C_1 and C_2 and the two halves of the inductor L form an LC bridge whose output is proportional to the difference between the two capacitances.

$\omega_{\rm out}^2 = 1/[(C_1 + C_2)L_{\rm out}]$ we must have $L_{\rm out} \simeq L/4$. Since the system has a bad heat dissipation, the amplitude of the signal should not exceed, say, 1 Volt in order to reduce power dissipation. We set $V_{\rm in}(t) = V_\circ \cos\omega_{\rm in} t$ with $V_\circ = 1\,{\rm Volt}$. The two capacitors of the bridge C_1 and C_2 are shown in Fig. 15. The signal is applied to the plates and the test

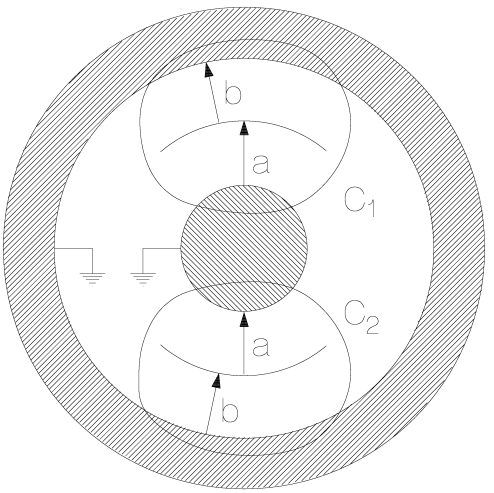

Fig. 15. Each capacitor of the read-out system (see also Fig. 16) is formed by two surfaces, one for each of the two grounded masses, and one plate, to which a sinusoidal voltage is applied. Any differential displacement of the test masses with respect to the plates causes a loss of balance of the system and therefore an output signal.

masses are electrically grounded. Let us call a and b the initial distances from the plate to the inner and outer mass respectively, with $a \simeq b$. If a and b are small a simplified analysis can be carried out assuming zero curvature parallel plates, and the initial values of the capacity are then $C_1^\circ = C_2^\circ \equiv C_\circ = \epsilon_\circ S(1/a + 1/b)$ (where $\epsilon_\circ$ is the dielectric constant of vacuum). In the cylindrical geometry the algebra is somewhat more complicated but with no relevant changes in the results. Any displacement of the test masses will change a ,b into a_1 ,b_1 for C_1 and a_2 ,b_2 for C_2. Such a displacement is the combination of a common mode and a differential mode displacement $\Delta x_{\text{c.m.}}$, $\Delta x_{\text{d.m.}}$ (Fig. 16). Because of $\Delta x_{\text{c.m.}}$ the values of the capacity change into

$$C_1 = \epsilon_\circ S\left(\frac{1}{a - \Delta x_{\text{c.m.}}} + \frac{1}{b + \Delta x_{\text{c.m.}}}\right)$$

$$C_2 = \epsilon_\circ S\left(\frac{1}{a + \Delta x_{\text{c.m.}}} + \frac{1}{b - \Delta x_{\text{c.m.}}}\right) \tag{46}$$

and therefore $(C_1 - C_2)_{\text{c.m.}}/(2C_\circ) \simeq (a - b)/(ab) \cdot \Delta x_{\text{c.m.}}$. Similarly for $\Delta x_{\text{d.m.}}$ we have:

$$C_1 = \epsilon_\circ S\left(\frac{1}{a - \Delta x_{\text{d.m.}}} + \frac{1}{b - \Delta x_{\text{d.m.}}}\right)$$

$$C_2 = \epsilon_\circ S\left(\frac{1}{a + \Delta x_{\text{d.m.}}} + \frac{1}{b + \Delta x_{\text{d.m.}}}\right) \tag{47}$$

hence, $(C_1 - C_2)_{\text{d.m.}}/(2C_\circ) \simeq -(a^2 + b^2)/[ab(a + b)] \cdot \Delta x_{\text{d.m.}}$. For the general displacement the total change of capacitance will be given by:

$$\frac{C_1 - C_2}{2C_\circ} \simeq \frac{a - b}{a^2}\Delta x_{\text{c.m.}} - \frac{1}{a}\Delta x_{\text{d.m.}} \tag{48}$$

which at resonance determines the output signal through the relation:

$$V_{\text{out}} = V_{\text{in}} \frac{C_1 - C_2}{2(C_1^\circ + C_2^\circ)} \cdot Q_{\text{out}} \tag{49}$$

where Q_{out} is the electrical quality factor of the output circuit. For instance, if $a = b \simeq 5\,\text{mm}$, $V_\circ = 1\,\text{V}$, $C_\circ \simeq 100\,\text{pF}$ and $Q_{\text{out}} \simeq 20$ we get $(C_2 - C_1)/(2C_\circ) \simeq \Delta x_{\text{d.m.}}/a \simeq 4.2 \cdot 10^{-10}$ and $V_{\text{out}} \simeq 4.2\,\text{nV}$, given the requirement to be sensitive to an EP displacement with $\eta = 10^{-16}$(Section 2.1) to a 95% confidence level, i.e. $1.05 \cdot 10^{-10}\,\text{cm}$. As for the thermal noise, laboratory tests have yielded:

$$\frac{\Delta C_N}{\sqrt{\text{Hz}}} \simeq 10^{-7}\,\frac{\text{pF}}{\sqrt{\text{Hz}}} \tag{50}$$

and therefore, since $\Delta a \simeq (a/2)\delta C/C$, the differential displacement Δa_N due to thermal noise is:

$$\frac{\Delta a_N}{\sqrt{\text{Hz}}} \simeq 3 \cdot 10^{-10}\,\frac{\text{cm}}{\sqrt{\text{Hz}}} \tag{51}$$

This means that the measurement accuracy required

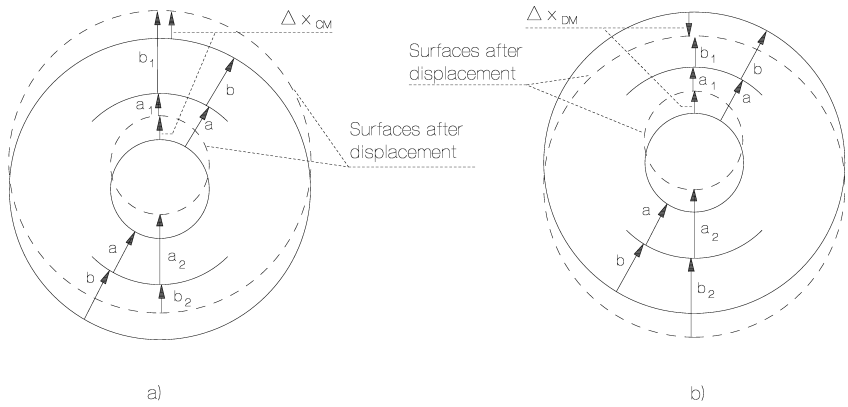

Fig. 16. The surfaces of the capacitors before and after: a) a common mode displacement and b) a differential mode displacement.

by the experiment can be achieved with an integration time of about 1 s. Thus, it is ruled out for the GG experiment be limited by the performances of the capacitance read out. Care should be taken in keeping parasitic capacitances small. However, since they depend on the geometry of the system, the resulting perturbation will be DC. It is therefore enough to make sure that their effect does not exceed the sensitivity by several orders of magnitude. It must be stressed that the required accuracy of $\simeq 1.05 \cdot 10^{-10}$ cm refers to relative displacements – at the spin frequency – of the centres of mass of the test bodies, not to their surface irregularities. The latter will only give DC effects.

It is apparent from Eq. (48) that for the read out to be sensitive to the displacement caused by a possible EP violation of $\eta = 10^{-16}$ the corresponding (differential) signal must be larger than the signal due to the largest possible displacement in common mode. Namely:

$$\frac{a-b}{a} \leqslant \frac{\Delta x_{\mathrm{EP}}}{\Delta x_{\mathrm{c.m.}}} \tag{52}$$

where $\Delta x_{\mathrm{EP}} \simeq 2.10 \cdot 10^{-10}$ cm and the maximum common mode displacement is due to air drag and amounts to $\simeq 5.3 \cdot 10^{-4}$ cm. Hence, the system must be balanced to $(a-b)/a \simeq 4 \cdot 10^{-7}$, which means $a - b \simeq 2 \cdot 10^{-7}$ cm = 20 Å. This level of balancing can be achieved actively by means of inch-worm piezoelectric actuators (Fig. 17) acting on the mechanical support of each capacitance plate to make their distance from the test masses as equal as possible. Inch-worm actuators are made of a combination of piezoceramics (no magnets) and can achieve relatively large displacements by a succession of very fine steps. Two inch-worms are needed for each plate, as shown in Fig. 2. The driving signal for this active balancing is a constant voltage obtained by a proper analysis of the 5 Hz signal. There is no danger to cancel an EP violation signal by actually making a and b different because the largest common mode effect – which is due to air drag – is variable in time. In any case, a phase check is able to tell whether the signal is due to air drag or EP violation. Inch-worms with 1 Å stepsize are commercially available.

We now consider the electrostatic force which affects each test mass. Let's take the inner test mass in the concentric initial configuration of Fig. 15. As the mass moves by an amount x it is subject to an average force $F(x)$ given by:

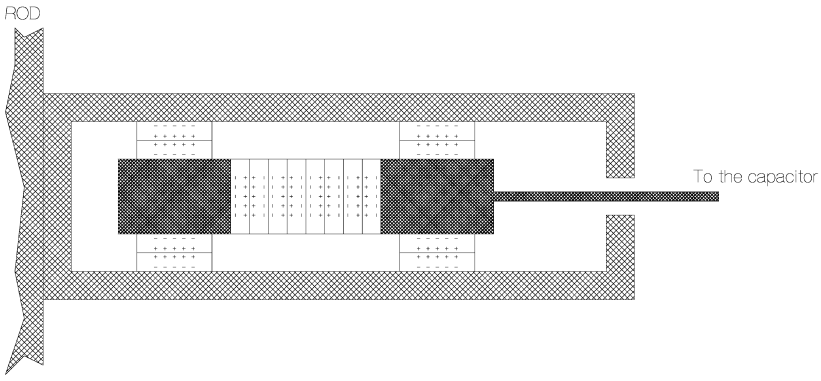

Fig. 17. Scheme of the inch-worm. Lateral piezoelectric actuators alternately fasten and release the extremities of the inch-worm to the sides of its container while the inner part is made to expand and contract by means of the other piezoelectrics. In this way the inch-worm can move on a relatively long path in successive very small steps.

$$\overline{F(x)} = \frac{1}{4}V_\circ^2\epsilon_\circ S\left[\frac{1}{(a-x)^2} - \frac{1}{(a+x)^2}\right] = \frac{1}{4}V_\circ^2\epsilon_\circ S\frac{x}{a^3} \quad (53)$$

This means that the electric forces simulate a spring with a negative constant k'

$$k' = -\frac{1}{4}V_\circ^2\epsilon_\circ S\frac{1}{a^3} \quad (54)$$

which could in principle be used to increase the displacement produced by the signal and to reduce the natural frequency of the test masses, which would in turn reduce the integration time because of the smaller thermal noise effect (Section 6.2). However, since the coupled suspension of the test masses with gimbals appears to give a rather low natural frequency this possibility needs not to be exploited.

Although a more detailed analysis is needed we conclude that a capacitance read out system can reach the required precision of 10^{-10} cm (corresponding to a 95% confidence level in the displacement due to an EP violation with $\eta = 10^{-16}$) in a very short time and is therefore by far adequate to the task. It is also worth stressing that ground tests of the capacitance read out system are possible, not only for the sensitivity of the circuit, but also for the balancing and corresponding reduction of the common mode displacements. We are working on a laboratory experiment with concentric, cylindrical test masses in high speed supercritical rotation and a capacitance read out like the one envisaged for GG. It would be a ground test of the main components of the space experiment as well as, possibly, a valuable EP experiment in its own right.

8. Coupling to higher mass moments of the test bodies

Test bodies are neither point like nor spherical. Therefore any source mass (e.g. the Earth and the spacecraft body) will interact with their mass moments (higher than the monopole) giving rise to differential effects between test masses. In the case of the Earth, because of the ω rotation of the test masses and the sensors, the effect will have this frequency, just like an EP violation. On the contrary, when the source is an unbalanced spacecraft mass the effect is DC because both the source and the test mass spin at the same rate. Let us compute the quadrupole acceleration due to the Earth (regarded as a point mass) on a test body in the shape of hollow cylinder with inner radius a, outer radius b, height L, a fractional difference $\Delta J/J_t = (J_p - J_t)/J_t$ between its principal moments of inertia and the symmetry axis at an angle θ with respect to the normal to the orbit plane (θ at most a few degrees). We get:

$$a_{\mathrm{qp}}^{\oplus} = \frac{3}{8}\frac{GM_{\oplus}}{R^2}\cdot\left(\frac{a^2 + b^2 + L^2/3}{R^2}\right)\frac{\Delta J}{J_t}\cdot f(\theta) \quad (55)$$

in the plane of symmetry of the cylinder (the effect along the symmetry axis is from 10 to 100 times smaller). The function $f(\theta)$ is about 1 for small θ. For two concentric test cylinders of equal mass, the dimensions and $\Delta J/J_t$ will be in general different, thus giving rise to a differential effect in competition with an EP violation signal. We have checked that in the 3-chamber setup of Fig. 1 which was used for the finite element numerical stability analysis presented in Section 3 (equal composition bodies in the central chamber, different composition bodies in the others) the resulting value of the quadrupole acceleration given by Eq. (55) is *for all bodies* at least one order of magnitude smaller than the expected signal $a_{\mathrm{EP}} \simeq 8.4\cdot 10^{-14}\,\mathrm{cm\,s^{-2}}$. Evidently, their differences in each chamber will also be below the signal. We therefore did not devote any effort to making the numerical value of the quantity $(a^2 + b^2 + L^2/3)\cdot \Delta J/J_t$ equal for the two masses. It is worth noticing that the values of $\Delta J/J_t$ (see Table 1) are not too small (from a few percents to 0.17) in order to avoid additional instabilities.

As for the interaction of an unbalanced mass of the spacecraft with the quadrupole moment of a test body, we note that despite a much smaller source

mass this effect is in fact larger because of its dependence on the fourth inverse power of the distance. However, it is constant because of the spinning of both the spacecraft and the test masses at the same frequency.

9. Electrostatic and magnetic effects

In any small force gravitational experiment electric charges on the test bodies must be absolutely avoided since they can easily produce forces far much bigger than the gravitational signal. The GG spacecraft does not contain free floating masses, and therefore no electrostatic charges will be able to build up inside it. Potential differences between the test masses can be avoided by coating them with a thin layer of the same conductive material. The PGB laboratory can be made of *Cu*, or another highly conductive material, so as to work as a Faraday cage, shielding the experiment from external electric fields. Any small residual charge inside the spacecraft will only produce a constant effect on the output signal and can therefore be neglected. It is worth stressing that this is a very important advantage of GG as compared to STEP, where the test bodies are suspended by means of magnetic bearings and the problem of discharging them without producing unwanted perturbations is a serious one. The problem is even worse if the spacecraft orbit goes, as in the case of STEP, through the Van Allen belts and is subject to the bombardment of charged particles in the so-called South Atlantic Anomaly. The orbit of GG is equatorial and at a low enough altitude to avoid the South Atlantic Anomaly.

Magnetic disturbances can be of two types: interactions of magnetized or magnetizable materials between themselves and interactions between these materials and the Earth's magnetic field. All magnetic and especially ferromagnetic materials inside the spacecraft should be avoided, i.e. magnets, electromagnets and electric motors. All electric currents should flow in shielded cables. For small controlled displacements we shall use piezoelectric actuators and active damping will be realized with

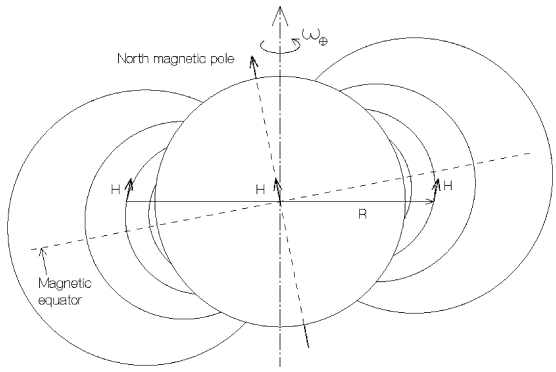

Fig. 18. In an equatorial orbit the direction of the Earth's magnetic field is not more than about 11° away from the perpendicular to the orbit. Therefore its effects in the plane of the orbit will be reduced to about $\sin 11° \simeq 0.2$ times those of the full field. These effects are distinguishable from a violation of the equivalence principle because they change sign every half orbit.

electrostatic actuators. Any residual constant magnetization inside the spacecraft, as for the case of electrostatic charges, would produce only a DC effect (unless there is a relative motion at the spinning frequency). If the GG satellite is essentially non magnetic, its attitude is almost unaffected by the Earth's magnetic field $\boldsymbol{H}$ because on average over one orbit $\boldsymbol{H}$ is almost parallel to the spin axis. Along the satellite orbit the instantaneous orientation of $\boldsymbol{H}$ is no more than about 11° away from the spin axis of the satellite (Fig. 18). Thus, the component of $\boldsymbol{H}$ in the orbit plane can only produces a signal whose amplitude is reduced by a factor $\sin(11°) \simeq 20\%$. If the interaction is between the proper test mass magnetization and the Earth's magnetic field, the frequency of this signal is $\omega - 2\pi/1^d$, because the shape of the magnetic field rotates with the Earth. The signal also changes sign every half orbit of the satellite. When the interaction is between induced magnetization on the test mass and the Earth's magnetic field, the frequency is $2(\omega - 2\pi/1^d)$ because it depends on H^2. We can argue in the same way for the component of $\boldsymbol{H}$ parallel to the spin axis. The interaction between magnetized test masses gives an $\omega - 2\pi/1^d$ signal only if the interaction is between an induced magnetized test mass and a test

mass with its own magnetization. A signal at this frequency could also arise if the test masses have their own magnetization and are subject to deformations (e.g. due to nonuniform thermal expansion) at the ω frequency.

Let us now estimate the intensity of these perturbations. The most dangerous ones are those which act at (or close to) the spin/signal frequency. The largest among them is due to the interaction between the magnetic moment μ_2 (due to ferromagnetic impurities) of one test body and the magnetization induced on the other (with susceptibility χ_1) by the magnetic field of the Earth. In the worst case hypotheses the resulting perturbing force which competes with the signal is (in MKS):

$$F_\omega \simeq V_1 \frac{\chi_1 B \sin\theta}{r^4} \mu_2 \tag{56}$$

with $B = \mu_\circ H \simeq 5 \cdot 10^{-5}\,\mathrm{T}$ ($\mu_\circ = 4\pi \cdot 10^{-7}\,\mathrm{V\,s/A\,m}$ the permeability of vacuum), $\theta \simeq 11°$, $r \simeq 0.05\,\mathrm{m}$ the mutual distance and $V_1 \simeq 10^{-3}\,\mathrm{m}^{-3}$ the volume of body 1. For it to be smaller than the signal $F_{\mathrm{EP}} \simeq 8.4 \cdot 10^{-15}\,\mathrm{N}$ it must be:

$$\chi_1 \mu_2 < 5.5 \cdot 10^{-12}\ \mathrm{A\,m^2} \tag{57}$$

Since reasonable values for the susceptibility are 10^{-6}, we need $\mu_2 < 5.5 \cdot 10^{-6}\,\mathrm{A\,m^2}$. From experimental data reported in textbooks we find that the magnetic moment of a cube of magnet of 0.01 cm size is about $5 \cdot 10^{-7}\,\mathrm{A\,m^2}$. Since this is in fact quite a large impurity, it appears that the inequality (Eq. (59)) can be satisfied by the test bodies thus ruling out any need of reducing the magnetic field of the Earth inside the satellite. Another magnetic perturbation which acts at the spin/signal frequency is due to the interaction of the magnetic moment of one test body with the magnetic field of the Earth. Worst case hypotheses give:

$$F'_\omega \simeq \mu_2 \frac{B}{R} \sin\theta \tag{58}$$

hence we need $\mu_2 < 6 \cdot 10^{-3}\,\mathrm{A\,m^2}$, which can be easily satisfied. A DC magnetic perturbation comes from the interaction of the magnetic moments of two test bodies with one another:

$$F_{\mathrm{DC}} \simeq \mu_\circ \frac{\mu_1 \mu_2}{r^4} \tag{59}$$

For it to be smaller than the signal it must be $\mu_1 \simeq \mu_2 < 2 \cdot 10^{-7}\,\mathrm{A\,m^2}$, which, from the previous discussion, is a reasonable requirement for a DC effect. We complete the analysis by estimating the magnetic perturbations which contain B^2 and therefore appear at a frequency close to twice the spin/signal frequency. One of these effects is due to the interaction of the magnetic moments induced on the test bodies with one another:

$$F_{2\omega} \simeq \frac{1}{\mu_\circ} V_1 V_2 \chi_1 \chi_2 \frac{B^2}{r^4} \sin\theta^2 \tag{60}$$

which requires $\chi_1 \chi_2 < 7.3 \cdot 10^{-10}$ and is satisfied because $\chi \simeq 10^{-6}$. Another 2ω effect comes from the interaction between B and the magnetization induced on a test body by B itself. The resulting perturbation force is:

$$F'_{2\omega} \simeq \frac{\chi_1 V_1}{\mu_\circ} \frac{B^2}{R} \sin\theta^2 \tag{61}$$

and it is smaller than the signal provided that $\chi_1 < 0.8$, which is surely the case.

In conclusion, as far as magnetic perturbations in the GG experiment are considered, we have demonstrated that the only one which sets a somewhat demanding requirement is due to the coupling of the magnetic field of the Earth with the magnetic moment of either test body due to residual ferromagnetic impurities. For this effect to be neglected we need the magnetic moment of the test bodies not to exceed a few $10^{-6}\,\mathrm{A\,m^2}$, which appears to be feasible. On the contrary, in the torsion balance of the Eöt-Wash experiment (Su, 1992; Su et al., 1994) the magnetic field of the Earth near the balance was reduced by a total factor of 10^5 (partly with μ-metal shielding, partly with Helmotz coils). This seems to contradict our previous conclusion, especially if one considers that they have reached a sensitivity $\eta = 10^{-12}$ while the GG target is $\eta = 10^{-16}$. Indeed, it is not so and we are going to show why. The first important fact to bear in mind is that, despite its

higher target sensitivity the GG expected force signal is $\simeq 25$ times larger than it is in Eöt-Wash, because of the bigger EP signal in space and the larger mass of the test bodies. In GG there are two test bodies of 10 kg each while in the Eöt-Wash torsion balance there are 4 masses of 10 g each; the force signals are $\simeq 8.4 \cdot 10^{-15}$ N and $\simeq 3.4 \cdot 10^{-16}$ N respectively. Note that the force, not the acceleration, is relevant when dealing with nongravitational perturbations. Secondly, since the Eöt-Wash experiment is a torsion balance experiment it is sensitive to torques, hence also to the magnetic torque generated by the interaction of the magnetic field of the Earth with magnetic moments of the test bodies (due to residual ferromagnetic impurities). Indeed, it turns out that the magnetic moment of the tray on which the test bodies are positioned gives an even larger perturbation than the test masses themselves. For this torque to be smaller than that due to an EP violation it must be:

$$\mu_{\text{tray}} B < 3.4 \cdot 10^{-16} \cdot 0.03 \text{ Nm} \tag{62}$$

where $\simeq 0.03$ m is the length of the arm. It must therefore be $\mu_{\text{tray}} < 2 \cdot 10^{-13}$ A m^2 (having used $B = 5 \cdot 10^{-5}$ T as above, although the value used by Su et al. (1994) is actually $B = 3 \cdot 10^{-5}$ T). From measurement of the torsion angle in absence of any shielding or coils the Eöt-Wash group finds that the residual magnetic moment of the tray (made of Al) is $\simeq 2.4 \cdot 10^{-8}$ A m^2 (Su, 1992; Su et al., 1994), thus making a reduction of B by 10^5 crucial for the success of the experiment. This is achieved by means of a 3-layer μ-metal shielding for a factor 3 600 and of Helmotz coils for a factor 28. As for the Eöt-Wash test masses, the measured value of the residual magnetic moment is $\simeq 4 \cdot 10^{-10}$ A m^2 while the requirement imposed by the magnetic torque is about $7 \cdot 10^{-9}$ A m^2; with a factor 10^5 of reduction of the magnetic field of the Earth made necessary by the tray, this effect is no problem. The magnetic dampers, used to kill the swing and wobble modes so that the motor can provide a smooth rotation, will also benefit of the reduction of the magnetic field. In GG we have symmetric and concentric masses and the signal is a force, not a torque, thus we have nothing like the torque (Eq. (62)); we do not have any motor or magnetic dampers either.

10. Initial unlocking in supercritical rotation

All space experiments which involve freely falling or softly suspended bodies require them to be locked during launch, and properly unlocked once in orbit to start the experiment. First of all we find it important to avoid any danger of the payload hitting the spacecraft walls. This is done simply by having each suspended mass and the PGB laboratory constrained to only slight movements by means of mechanical stops. Gaps of a few millimetres in size make the very soft mechanical suspension dominate during the experimental phase but at the same time constrain the body to within a small range of movements in case anything unpredictable should happen. As for the launch phase, when the system is subject to strong accelerations, we envisage having a static mechanical locking for each body, typically made of 3 lockers 120° apart on each suspension side. As for the forces acting on the springs themselves during launch, we recall that their mass is very small; it is also possible to use mechanical stops in order to avoid large displacements. Estimates show that there is no danger for the elasticity regime to be exceeded during launch, even though some time for relaxation should probably be allowed at the beginning of the mission. Once the spacecraft has been injected in its orbit and given the required attitude and spin rate the static mechanical lockers can be released and never used again. A symmetrical locking consisting of 4 inch-worms placed at 90° from one another as shown in Fig. 19 is provided, each inch-worm being equipped with a force sensor sensitive to 1 dyn. It gives a measure of the centrifugal force in that direction, and therefore provides the driving signal to the inch-worms for reducing the distance offset from the rotation axis. Once this has been reduced to $\simeq 10^{-7}$ cm, which means a centrifugal force of $\simeq 1$ dyn for the suspended test masses, active centering with inch-worms can be stopped; the electrostatic

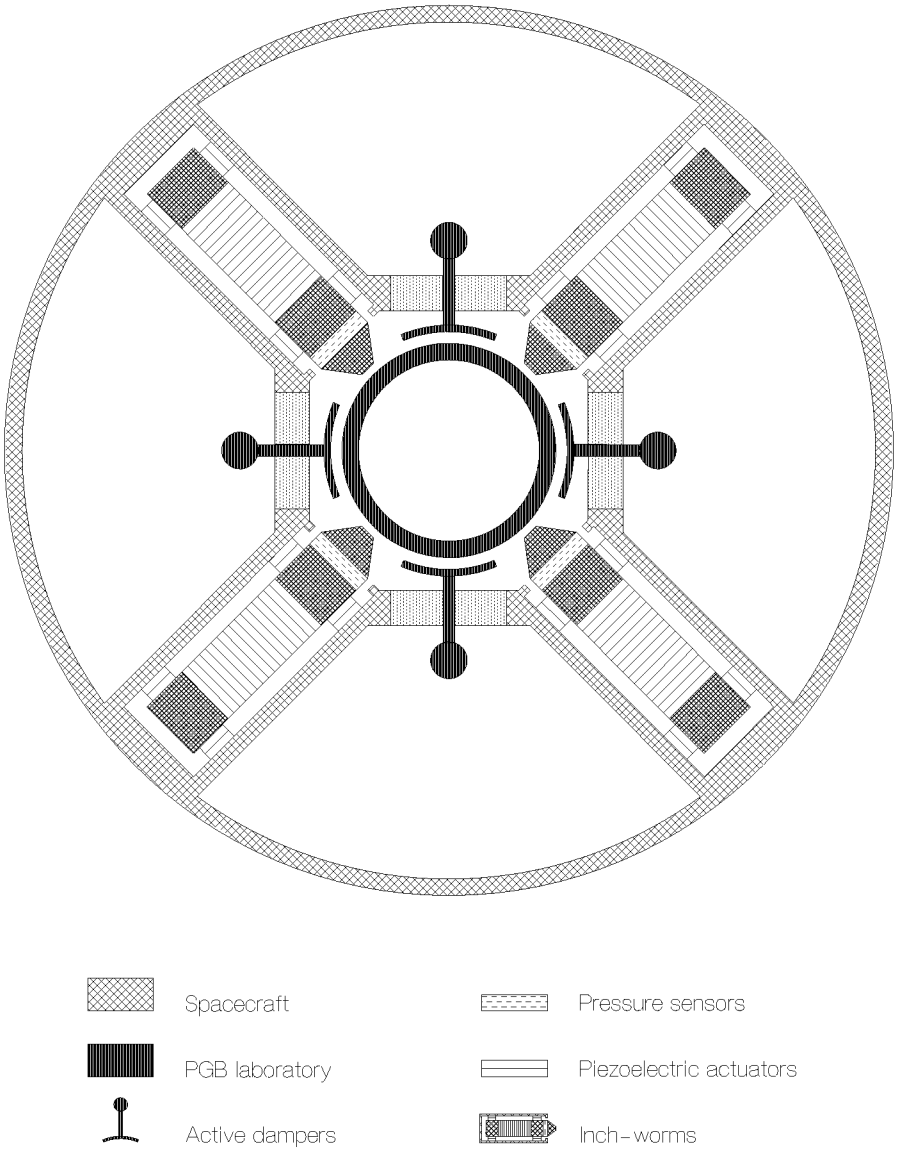

Fig. 19. Top view of a set of four inch-worms actuators for locking and unlocking the suspended masses. Each mass needs two such sets placed at its two axial ends (see also Fig. 2). Between the inch-worms are the electrostatic plates used for active damping. The rod, hence the suspended masses, is locked during launch and until the spacecraft has reached the final spin angular velocity ω. Then the inch-worms equipped with pressure sensors sensitive to $\simeq 1\,\mathrm{dyn\,cm^{-2}}$ are used for initial centering until the centrifugal forces detected by the pressure sensors become smaller than the forces that can be generated by the electrostatic plates. At this point the inch-worm will be retracted and the electrostatic system will complete the centering and will keep it stable.

dampers will then stabilize whirling and precessional motions around the equilibrium position of supercritical rotation as shown in Section 3. While the static lockers are meant not to be reused, the inchworms can. Together with the mechanical stops they make the system in principle safe from unexpected occurrences.

11. Conclusions

General Relativity and all metric theories of gravity rely on the principle of equivalence between inertial and gravitational mass. Its fundamental character and far reaching implications make it necessary for it to be tested as accurately as possible by testing the *Universality of Free Fall*. If the test bodies orbit around the Earth the signal is about 3 orders of magnitude bigger than at its surface, and this is what makes space experiments to test the equivalence principle so attractive despite their inevitable difficulties. We have presented here a nondrag-free version of the *Galileo Galilei (GG)* mission proposal, arguing that it could detect any deviation from the *Universality of Free Fall* – hence from the equivalence between inertial and gravitational mass – to the level of 1 part in 10^{16}, four orders of magnitude better than the most recent ground tests (Adelberger et al., 1990; Su et al., 1994). The main features of this concept are to be nondrag-free and non cryogenic, to make the test bodies spin at a relatively high frequency chosen by the experimentalist (e.g. 5 Hz) and to exploit the zero-*g* space environment in order to naturally obtain self-centering of the test bodies and a very low level of vibrational noise. The spacecraft is small, compact and essentially passive so as to minimize disturbances on the test masses; no active control, neither of the orbit nor of the attitude is needed. The signal from a violation of equivalence would be modulated at the spin frequency of the test bodies (and the spacecraft) while the common rotation of the entire apparatus makes many internal perturbing effects DC. The read out system is capacitive. In the perturbation analysis we have tried to keep all directly competing effects well below the target signal unless otherwise distinguishable. Thermal perturbations can be sufficiently reduced by passive insulation thanks to fast spin and vacuum. It is concluded that a violation of equivalence to the level of 1 part in 10^{16} can be detected with an integration time of a few hours. A partial compensation of air drag would help reduce the intensity of inertial forces on test bodies and – correspondingly – the required level of common mode rejection. However, drag-free control is advantageous only if the thrusters are proportional rather than impulsive and the propellant to be carried on board does not itself give rise to perturbations. An interesting possibility would be to use FEEP (Field Emission Electric Propulsion) thrusters, which need a negligible amount of Cesium and are meant to be highly proportional. A drag-free GG mission with FEEP thrusters (Nobili et al., 1995; GALILEO GALILEI, 1996) can indeed aim at a 1 order of magnitude better sensitivity, i.e. at an EP test to 1 part in 10^{17}. As for the possibility to run the experiment at low temperature, the advantages must be weighed against the disturbances due to the cryogenic system itself. Taking also into account that a room temperature capacitive read out is adequate to the task, we have preferred to consider a non cryogenic experiment. The choice for a space mission completely devoted to one single scientific objective (indeed the entire spacecraft, its orbit and attitude control are driven by this objective) was done on purpose, to reduce the complexity, cost and realization time were any space agency interested in the experiment. To this end it is worth stressing that the major components of the space experiment can be tested in the ground laboratory, and even though the entire apparatus is designed for zero *g* a modified, less accurate (due to the weaker signal), 1-*g* version of it is possible and is underway.

Acknowledgements

We are grateful to E.G. Adelberger, L. Anselmo, B. Bertotti, P.G. Bizzeti, V.B. Braginsky, A. Brillet, A. Di Virgilio, F. Fuligni, V. Iafolla, A. Milani, I.

Modena, P. Melchior, G. Pizzella, T. Quinn, P. Rapagnani, F. Ricci, E. Rossi and Y. Su for useful discussions and contributions. Special thanks are due to the Italian Space Agency (ASI) for primary financial support.

References

Adelberger, E.G., Stubbs, C.W., Heckel, B.R., Su, Y., Swanson, H.E., Smith, G., Gundlach, J.H., & Rogers, W.F., 1990, PhRvD, 42, 3267.

Barlier, F., Blaser, J.P., Cavallo, G., et al., 1991, in: STEP: Satellite Test of the Equivalence Principle, Assessment Study Report, ESA/NASA SCI (91) 4.

Bender, P., Brillet, A., Ciufolini, I., Danzmann, K., Hellings, R., Hough, J., Lobo, A., Sandford, M., Schutz, B., & Touboul, P., 1994, in: LISA: Laser Interferometer Space Antenna for gravitational waves measurements, ESA SCI (94) 5.

Beverini, N., Billen, J.H., Bonner, B.E., et al., 1986, CERN/PSCC/86-2 PSSC/P-64, Los Alamos National Laboratory Report LA-UR-86-260.

Blaser, J.P., Bye, M., Cavallo, G., et al., 1993, STEP: Satellite Test of the Equivalence Principle, Report on the Phase Study, A, ESA/NASA SCI (93) 4.

Blaser, J.P., Cruise, M., Damour, T., Leòn, J., Paik, H.J., & Rummel, R., 1994, STEP: Satellite Test of the Equivalence Principle. A Fundamental Physics Laboratory in Space, Assessment Study Report, ESA SCI (94) 5.

Blaser, J.P., Cornelisse, J., Cruise, et al., 1996, STEP: Satellite Test of the Equivalence Principle, Report on the Phase Study, A, ESA SCI (96) 5.

Braginsky, V.B., private communication, 1993.

Braginsky, V.B. & Panov, V.I., 1972, Sov. Phys. JEPT 34, 463.

Bramanti, D., Nobili, A.M., & Catastini, G., 1992, Phys. Lett. A 164, 243.

Bramanti, D., Nobili, A.M., & Catastini, G., 1996, Stabilization of Weakly Coupled Rotors: A General Derivation of the Required Forces.[14]

Cajori, F., 1934, Sir Isaac Newton's Mathematical Principles of Natural Philosophy and his System of the World (University of California, Berkeley, CA).

Cappellari, J.O., et al., 1976, Mathematical Theory of the Goddard Trajectory Determination System, GSFC X-582-76-77, Sections 4.5.6, 4.53–4.57.

Catastini, G., Bramanti, D., Nobili, A.M., Fuligni, F., & Iafolla, V., 1992, ESA Journal 16, 401.

Catastini, G., Nobili, A.M., & Bramanti, D., 1996, Passive Vibration Isolation in a Spinning Spacecraft.[15]

Chapman, P.K. & Hanson, A.J., 1970, Proceedings of the Conference on Experimental Tests of Gravitational Theories, Cal. Tech. JPL TM No. 33-499, p. 228.

Den Hartog, J.P., 1985, Mechanical Vibrations (Dover Publications, Inc., New York, first published 1934).

Ducarme, B., 1994, private communication.

Eötvös, R.V., Pekar, D., & Fekete, E., 1922, Ann. Physik 68, 11.

Fishbach, E., Sudarsky, D., Szafer, A., Talmadge, C., & Aronson, S.H., 1986, Phys. Rev. Lett., 56, 3.

Galilei, G., 1638, Discorsi e Dimostrazioni Matematiche intorno a due Nuove Scienze Attinenti alla Meccanica e i Movimenti Locali, in: Barbèra G., eds. (Le Opere, Firenze, VIII., 1968) p. 116.

GALILEO GALILEI (GG), PRE PHASE A REPORT, ASI (Agenzia Spaziale Italiana, September 1996).

GALILEO GALILEI (GG), ADDENDUM No. 1 TO THE PRE PHASE A REPORT, ASI(Agenzia Spaziale Italiana, May 1997).[16]

Genta, G., 1993, Vibration of structures and machines (Springer, New York).

Harris, I. & Priester, W., 1952, Jour. Atmos. Sciences, 19, 4 (also NASA-TN-D-1443).

Harris, I. & Priester, W., 1962, Theoretical Models for the Solar Cycle Variation of the Upper Atmosphere, in: GSFC Report NASA-TN-D-144.

Haselden, G.G., ed., 1971, Cryogenic Fundamentals (Academic Press, London).

Immergut, B., ed., 1984, Polymer Handbook 2nd Ed. (J. Wiley & Sons, New York).

Jacchia, L.G., 1971, Revised Static Models of the Termosphere and Exosphere with Empirical Temperature Profiles, in: SAO Special Report No. 332 (Cambridge, MA).

Jeffcott, H.H., 1919, Philos. Mag. Series 6, 37, 34.

Melchior, P., 1978, The Tides of the Planet Earth (Pergamon, Oxford).

Melchior, P., Barlow, B., Ducarme, B., & Delcourt, M., 1979, Discussion of a Long Series of Gravity Tide Measurements at Alice Springs in the Centre Australia, in: IUGG Gen. Assembly, Symp. 20 (Canberra, ACT).

Milani, A., Nobili, A.M., & Farinella, P., 1987, Non-Gravitational Perturbation and Satellite Geodesy (Adam Hilger, Bristol).

Nobili, A.M., Milani, A., Polacco, E., Roxburgh, I.W., Barlier, F., Aksnes, K., Everitt, C.W., Farinella, P., Anselmo, L., & Boudon, Y., 1990, ESA Journal, 14, 398.

Nobili, A.M., Catastini, G., Di Virgilio, A., Iafolla, V., & Fuligni, F., 1991, Phys. Lett. A, 160, 45.

[14]http://adams.dm.unipi.it/ñobili/ggweb/pap1/pap1.html

[15]http://adams.dm.unipi.it/ñobili/ggweb/pap2/pap2.html

[16]http://adams.dm.unipi.it/ñobili/ggweb/addendum/addendum.html

Nobili, A.M., Bramanti, D., Polacco, E., et al., 1994, Proposed New Test of the Equivalence Principle in Space, PISA Preprint on Astrophysics and Space Mechanics (Revised February 1995).[17]

Nobili, A.M., Bramanti, D., Catastini, G., et al., 1995, J. Astronautical Sciences, 43, 219.

Nobili, A.M., Bramanti, D., Catastini, G., Anselmi, A., Portigliotti, S., Lenti, A., Volpi, G., & Marcuccio, S., 1996, Galileo Galilei (GG) – Test of the Equivalence Principle with a small Spinning satellite: The Stabilization of its Weakly Coupled Masses, in: Scientific Satellites Achievements and Prospects in Europe, Proceedings AAAF–ESA 3.74.

Park, J.W., 1990, PhD Thesis (University of Maryland).

Quinn, T.J., 1993, private communication.

Roberts, Jr., E.R., 1971, Celest. Mech. 4 (3/4), 368.

Roll, P.G., Krotkov, R., & Dicke, R.H., 1964, Ann. Phys. (NY) 26, 442.

Sanders, A.J. & Deeds, W.E., 1992, PhRvD, 46, 489.

Scherk, J., 1979, Phys. Lett. B 88, 265.

Su, Y., 1992, PhD Thesis (University of Washington).

Su, Y., Heckel, B.R., Adelberger, E.G., Gundlach, J.H., Harris, M., Smith, G.L., & Swanson, H.E., 1994, PhRvD, 50, 3614.

Whitley, S., 1984, Rev. Mod. Phys., 56, 67.

Will, C.M., 1992, Int. J. Mod. Phys. D, 1, 13.

Worden, Jr., P.W., 1976, PhD thesis (Stanford University).

Worden, Jr., P.W., 1987, Acta Astronautica, 5, 27.

Worden, Jr., P.W. & Everitt, C.W.F., 1973, Proceedings Int. School of Physics E. Fermi, Course LVI: Experimental Gravitation (Academic Press, New York), p. 381.

Worden, Jr., P.W., Everitt, C.W.F., & Bye, M., 1990, Satellite Test of the Equivalence Principle, Science Requirements Document (Stanford University).

[17] http://adams.dm.unipi.it /publications/gg.ps.gz